

Solving the homogeneous Bethe-Salpeter equation with a quantum annealer

Filippo Fornetti¹, Alex Gnech^{2,†}, Tobias Frederico³, Francesco Pederiva⁴, Matteo Rinaldi⁵,
Alessandro Roggero⁴, Giovanni Salmè⁶, Sergio Scopetta^{1,*} and Michele Viviani⁷

¹*Dipartimento di Fisica e Geologia, Università di Perugia, and INFN, Sezione di Perugia,
Via Alessandro Pascoli, 06123 Perugia, Italy*

²*Department of Physics, Old Dominion University, Norfolk, Virginia 23529, USA and Theory Center,
Jefferson Laboratory, Newport News, Virginia 23606, USA*

³*Instituto Tecnológico de Aeronáutica, 12228-900 São José dos Campos, Brazil*

⁴*Dipartimento di Fisica, Università di Trento, and INFN-TIFPA, Via Sommarive 14,
Povo 38123, Trento, Italy*

⁵*INFN, Sezione di Perugia, Via Alessandro Pascoli, 06123 Perugia, Italy
and Dipartimento di Fisica e Geologia, Università di Perugia, Italy*

⁶*INFN, Sezione di Roma, Piazzale Moro 2, 00185 Rome, Italy*

⁷*INFN, Sezione di Pisa, Largo Pontecorvo 3, 56100, Pisa, Italy*

 (Received 28 June 2024; accepted 7 August 2024; published 6 September 2024)

The homogeneous Bethe-Salpeter equation (hBSE), describing a bound system in a genuinely relativistic quantum-field theory framework, was solved for the first time by using a D-Wave quantum annealer. After applying standard techniques of discretization, the hBSE, in ladder approximation, can be formally transformed in a generalized eigenvalue problem (GEVP), with two square matrices: one symmetric and the other nonsymmetric. The latter matrix poses the challenge of obtaining a suitable formal approach for investigating the *nonsymmetric* GEVP by means of a quantum annealer, i.e., to recast it as a quadratic unconstrained binary optimization problem. A broad numerical analysis of the proposed algorithms, applied to matrices of dimension up to 64, was carried out by using both the PROPRIETARY simulated-annealing package and the D-Wave *Advantage 4.1 system*. The numerical results very nicely compare with those obtained with standard classical algorithms, and also show interesting scalability features.

DOI: [10.1103/PhysRevD.110.056012](https://doi.org/10.1103/PhysRevD.110.056012)

I. INTRODUCTION

The past decade has seen an exponential growth of research activity and interest in quantum computing in an impressive number of fields (see, e.g., Refs. [1–11] for recent reviews which could offer an admittedly partial idea of the state-of-the-art). The driving force behind all of this has been the astonishing advances in new quantum-hardware implementation which occurs with close frequency, as shown by the long list of major achievements one can find in literature and media (see, e.g., Ref. [12] for an introduction of the main quantum-computing platforms, as well as algorithms). However, one should recall

that an easy path toward a universal, fault-tolerant quantum computer is currently hindered by noise, decoherence and scalability [1].

In general, one can perform calculations that take advantage of either digital gate-based quantum computing or analog quantum annealing (see, e.g., Ref. [13] for a detailed discussion of the two approaches). The first choice is more widely adopted, since it is meant as the quantum analog of a classical general-purpose computer, and it has the possibility to address a broader set of problems (see, e.g., Ref. [14], for recent experimental results obtained using an IBM quantum machine). The second possibility, the quantum annealing, is mainly devoted to optimization problems, that can be properly encoded into an Ising Hamiltonian. In this case, one searches for the ground-state of the system by exploiting quantum fluctuations (see, e.g., Refs. [15–19] for an introduction to the foundations of quantum annealing). Quantum annealing, that has its basis in the adiabatic theorem, have been exploited in several practical applications (see, e.g., Refs. [20–24] and references quoted therein for a nonexhaustive list of quantum-annealing

*Contact author: sergio.scopetta@esteri.it
Present address: Science Counsellor at the Italian Embassy in Spain, calle Lagasca 98, 28006 Madrid, Spain.

†Contact author: agnech@odu.edu

Published by the American Physical Society under the terms of the [Creative Commons Attribution 4.0 International license](https://creativecommons.org/licenses/by/4.0/). Further distribution of this work must maintain attribution to the author(s) and the published article's title, journal citation, and DOI. Funded by SCOAP³.

applications) outperforming the results obtained with simple classical heuristics, like simulated annealing.

In this work we exploit this second possibility to solve the *nonsymmetric* generalized eigenvalue problem (GEVP). In particular we use the D-Wave Advantage quantum annealer (QA) [25–27] which has a network of more than 5000 qubits, with 15-way connectivity.

The application of the quantum annealer for finding the solution of the GEVP for *symmetric* matrices it is very well known in literature [28–32]. In this work, we aim instead to find the minimal/maximum right eigenvalue (and corresponding eigenvector) of a *nonsymmetric* GEVP by the use of a quantum annealer. Notice that the proposed technique could also be used for the left eigenvectors with simple modifications. In our specific case we focus on the *nonsymmetric* GEVP stemming from the discretization method adopted for solving the homogeneous Bethe-Salpeter equation (hBSE) [33,34] in ladder approximation, directly in the four-dimensional (4D) Minkowski space (see also Refs. [35–37] for a detailed introduction to the topic, and the brief resumé in Appendix A). In particular we focus on the numerical solutions of the hBSE for two massive scalar fields interacting through the ladder exchange of another massive scalar field (see Ref. [38] for the results obtained with a classical computation).

The *nonsymmetric* GEVP is given in general by the expression

$$A\mathbf{v}_i = \lambda_i B\mathbf{v}_i \quad (1)$$

where the $n \times n$ matrix A is a real and *nonsymmetric*, the $n \times n$ matrix B is nonsingular and *symmetric* and, \mathbf{v}_i is the eigenvector corresponding to the i th eigenvalue λ_i . It is important to underline that this form is relevant for many areas, e.g., for the analysis of mechanical systems [39,40], in fluid mechanics [41], for investigating criticality in nuclear reactors [42] or the onset of oscillatory instability in a heated cavity [43], for lattice QCD [44], in industry [45], etc.

At the present stage, we reduce the GEVP into a standard eigenvalue problem by inverting the matrix B through a classical algorithm, before passing it to the quantum annealer to compute the real maximal/minimal eigenvalue and eigenvector. This is a crucial first step of the investigation since it permits to assess the viability of this algorithm before being generalized.

The problem is then divided in two steps. The first step is to translate the GEVP into a quadratic unconstrained binary optimization¹ (QUBO), constructing the suitable *objective function* (OF) in terms of binary variables. The second step, carried out through the PROPRIETARY software, is to map the QUBO problem onto such Ising-model, embodied by the qubit architecture (see Ref. [46] for the first implementation of a QUBO problem on a D-Wave QA and

Refs. [25–27] for the D-Wave Advantage System). The quantum annealer is then used to search for the global minimum of the corresponding Ising Hamiltonian implemented on the physical quantum processing units (QPUs).

The paper is organized as follows. In Sec. II, the physics problem from where the *nonsymmetric* GEVP stemmed from is briefly illustrated. In Sec. III, the OF, which our GEVP is mapped onto, and its expression in terms of the binary variables are presented in detail. In Sec. IV, the results of our numerical investigation on the annealing simulator, SA, as well as the D-Wave Advantage System QA are discussed at some length and compared. Finally, in Sec. V, our conclusions are drawn with a focus on the perspectives. Appendixes are devoted to supply more details on the physics case and the construction of the OF.

II. THE PHYSICS PROBLEM

As previously stated, our aim is to solve the homogeneous Bethe-Salpeter equation [33] of a system composed by two massive scalars bound through the ladder exchange of a third massive scalar, directly in Minkowski space. A variational method, tailored for a QA, is applied in order to obtain the ground-state of the system. This non-perturbative quantum-field-theory problem was solved in Ref. [38] by using the Nakanishi integral representation [47] (NIR) of the Bethe-Salpeter (BS) amplitude, i.e., the key quantity for describing the ground-state of the system and eventually calculating relevant observables. Following Ref. [38], one can formally transform the hBSE in Minkowski space into a GEVP adopting a standard discretization method. In particular, a polynomial orthonormal basis, composed by the Cartesian product of Laguerre and Gegenbauer polynomials, was adopted. It should be pointed out that solutions obtained directly in Minkowski space make a more direct comparison between the theoretical outcomes and the experimental results possible, without resorting to Euclidean solutions (see, e.g., Refs. [48–50] for an introduction to the Dyson-Schwinger plus hBSE framework, in Euclidean space). Let us recall that Euclidean solutions could be directly adopted for describing physical observables, once the assumptions of the famous theorems by Osterwalder and Schrader [51,52], stating necessary and sufficient conditions for formally bridging Euclidean and Minkowskian quantum-field theory, are fulfilled and the set of unavoidable approximations is actually under control.

From a bird’s eye view, the two-body BS amplitude allows to reconstruct the residue of the four-leg Green’s function at the bound-state mass pole. Moreover, one can show that such an amplitude is the solution of a homogeneous integral equation, i.e., the hBSE. Notice that, in relativistic quantum-field theory, the hBSE has the same role in the bound-state description that the Schrödinger equation has in nonrelativistic quantum mechanics.

In conclusion, one is able to formally transform the Minkowskian hBSE into the *nonsymmetric* GEVP of the

¹One aims to get a quadratic polynomial over binary variables.

form in Eq. (1). The eigenvalue is proportional to the inverse of the square coupling constant present in the interaction vertex (produced by the underlying field theory). Since the coupling constant is real for physical reasons, real eigenvalues must be sought. It should be pointed out that the eigenvalues and corresponding eigenvectors (eigenpair) in a *nonsymmetric* GEVP can be real or complex. In case they are complex they appear in conjugated pairs. Moreover, the eigenvectors \mathbf{v}_i do not have the property to be orthogonal. As specified above, in our case we are interested only in the real eigenvalues, and particularly the one corresponding to the largest, positive real λ_i , since it is the inverse of the minimal coupling constant that allows the existence of a bound system with a given mass [38].

III. QA MODELING OF A NONSYMMETRIC GENERALIZED EIGENVALUE PROBLEM

In order to perform numerical calculations on a QA, the actual problem has to be expressed as a QUBO model or, equivalently, to find an Ising-model form for the problem under scrutiny (see, e.g., Ref. [53] for a tutorial on formulating and using QUBO models).

For a symmetric GEVP, where the eigenvalues are real, there are already several investigations with specific application to different problems (see, e.g., Refs. [28–30,54–56]). In all these applications, the Rayleigh-Ritz variational principle is adopted to transform the eigenvalue problem in a QUBO form. For the *nonsymmetric* GEVP, involving also complex eigenpairs, dedicated efforts are still needed. Recalling that QUBO problems are by definition strictly symmetric, one should be able to replace the nonsymmetric original problem with a symmetric one, which allows to evaluate the set of real eigenpairs we are interested in. This will be achieved by transforming the initial GEVP into a symmetric one with an equivalent spectrum. Thus, the same algorithm used for applying the Rayleigh-Ritz variational principle, with minimal changes, can be adopted. In performing such a transformation, the minimization problem acquires a quadratic dependence on the parameter playing the role of eigenvalue. This means that each eigenvalue is a minimum. This on one side can be usefully exploited for addressing the entire spectrum on the other side require to guide the search toward the relevant region where the eigenvalue has to be found.

In this Section we go through the formalism we adopted for the nonsymmetric case with some detail.

A. Formalism

Since the physical case under consideration generates a nonsymmetric matrix A in Eq. (1), the Rayleigh-Ritz variational principle is not directly exploitable. A first trivial attempt to overcome this problem might be to single out the symmetric part of the matrix A , and solve the

corresponding symmetric GEVP, recalling that B by itself is symmetric. Unfortunately, this formal manipulation does not return the original global minimum. This is illustrated in Appendix C, where an inequality between the eigenvalues of a nonsymmetric matrix and the ones of its symmetric part is discussed in the simpler case of a standard eigenvalue problem. Therefore, the eigenvalue problem $[(A + A^T)/2]\mathbf{v}_i = \lambda_i B\mathbf{v}_i$ cannot be used for determining the minimal/maximal eigenvalue of Eq. (1). The same issue is met also for other methods of symmetrization, like $A^T A$ (see Appendix C for more discussion and examples).

A possible way to overcome this problem was discussed in Ref. [39], where the symmetrization of the original problem is recast as the product of $A - \tilde{\lambda}B$ with its transpose, i.e.,

$$S = [A^T - \tilde{\lambda}B^T][A - \tilde{\lambda}B], \quad (2)$$

where $\tilde{\lambda}$ can be complex (see below).

The resulting OF, which now contains a symmetric product, reads

$$\begin{aligned} f(A, B, \mathbf{v}, \tilde{\lambda}) &= \mathbf{v}^T [A^T - \tilde{\lambda}B^T][A - \tilde{\lambda}B]\mathbf{v} \\ &= \mathbf{v}^T [A^T A - 2\tilde{\lambda}M + \tilde{\lambda}^2 B^T B]\mathbf{v} \geq 0, \end{aligned} \quad (3)$$

where \mathbf{v} is chosen to be a *real* normalized vector and M is a symmetric matrix, defined as

$$M = \frac{(B^T A + A^T B)}{2}. \quad (4)$$

In what follows, it should be kept in mind that our goal is to find a real eigenpair of the analyzed GEVP, although the OF $f(A, B, \mathbf{v}, \tilde{\lambda})$ vanishes also for complex eigenpairs.

The striking difference between the global-minimum search of $f(A, B, \mathbf{v}, \tilde{\lambda})$ and the standard eigenvalue problem is the quadratic dependence upon the variable $\tilde{\lambda}$. Calling λ the solution of the quadratic form in Eq. (3) for a given real vector \mathbf{v} , one gets

$$\lambda(\mathbf{v}) = \lambda^R(\mathbf{v}) \pm i\lambda^I(\mathbf{v}) \quad (5)$$

where the real part is

$$\lambda^R(\mathbf{v}) = \frac{\tilde{M}(\mathbf{v})}{|B\mathbf{v}|^2}. \quad (6)$$

with $\tilde{M}(\mathbf{v}) = \mathbf{v}^T M \mathbf{v}$. The imaginary part is written as follows

$$\lambda^I(\mathbf{v}) = \frac{\sqrt{\mathcal{I}(\mathbf{v})}}{|B\mathbf{v}|^2} \quad (7)$$

where

$$\mathcal{I}(\mathbf{v}) = \|A\mathbf{v}\|^2 \|B\mathbf{v}\|^2 - \tilde{M}^2(\mathbf{v}), \quad (8)$$

with $\|A\mathbf{v}\|^2 = \mathbf{v}^T A^T A \mathbf{v}$ and equivalently for $\|B\mathbf{v}\|^2$. Notice that $\mathcal{I}(\mathbf{v})$ is a positive quantity, since

$$\begin{aligned} \mathcal{I}(\mathbf{v}) &= \|A\mathbf{v}\|^2 \|B\mathbf{v}\|^2 - \left[\mathbf{v}^T \frac{B^T A + A^T B}{2} \mathbf{v} \right]^2 \\ &\geq \|A\mathbf{v}\|^2 \|B\mathbf{v}\|^2 - \left[\frac{\|\mathbf{v}^T B^T A \mathbf{v}\| + \|\mathbf{v}^T A^T B \mathbf{v}\|}{2} \right]^2 \\ &\geq \|A\mathbf{v}\|^2 \|B\mathbf{v}\|^2 - \|\mathbf{v}^T B^T A \mathbf{v}\|^2 \geq 0. \end{aligned} \quad (9)$$

Therefore, our task is to set up an algorithm for finding a real vector \mathbf{v} that minimizes both the OF and the imaginary part of the eigenvalue, $\lambda^I(\mathbf{v})$, so that the set $\{\mathbf{v}, \lambda^R(\mathbf{v})\}$ is the searched eigenpair. Notice that a real vector \mathbf{v} that minimizes $\mathcal{I}(\mathbf{v})$, also minimizes the OF $f(A, B, \mathbf{v}, \tilde{\lambda} = \lambda^R)$. However, the opposite is not true, since the OF vanishes also for complex eigenpairs.

In Ref. [39], the search was carried out by classically minimizing $\mathcal{I}(\mathbf{v})$ through a gradient-descent method. Unfortunately, $\mathcal{I}(\mathbf{v})$ has a quartic dependence on \mathbf{v} , and therefore the corresponding minimization cannot straightforwardly be translated into a QUBO problem. The quartic problem can be recast into a quadratic one by adding suitable penalties, at the price of a substantial increase of the dimension of the QUBO problem (see, e.g., Refs. [53,57]). However this will require to substantially increase the matrix size to pass to the annealer. In order to overcome the difficulties, we approached the problem in a different way.

First of all, given the exploratory nature of our investigation, instead of directly using the OF in Eq. (3), we introduced a hybrid algorithm, namely, we transformed the initial GEVP into a standard one, leaving the generalized problem for future investigations. We exploit the symmetry and nonsingularity of the matrix B , decomposing it by using the standard LDL^T factorization, with L a lower triangular matrix, having diagonal elements equal to 1, and D a nonsingular diagonal matrix (see, e.g., the LAPACK library). Hence, the original GEVP, Eq. (1), becomes

$$CL^T \mathbf{v}_i = \lambda_i L^T \mathbf{v}_i, \quad (10)$$

where

$$C = D^{-1} L^{-1} A [L^T]^{-1}, \quad (11)$$

is nonsymmetric, and the real vector $L^T \mathbf{v}_i$ is no longer normalized. Since the global-minimum search is not affected by multiplicative factors, we can use a normalized vector formally defined by

$$\mathbf{w} = L^T \mathbf{v} / \|L^T \mathbf{v}\|. \quad (12)$$

Then, one can address the QUBO problem by replacing the initial OF with an equivalent one, given by

$$f(C, \mathbf{w}, \tilde{\lambda}) = \mathbf{w}^T [C^T - \tilde{\lambda}] [C - \tilde{\lambda}] \mathbf{w}. \quad (13)$$

The real part of the solution of the quadratic form in $\tilde{\lambda}$, for a given \mathbf{w} , is

$$\lambda^R(\mathbf{w}) = \frac{1}{\|\mathbf{w}\|^2} \mathbf{w}^T \frac{C^T + C}{2} \mathbf{w}, \quad (14)$$

while the imaginary part reads

$$\lambda^I(\mathbf{w}) = \sqrt{\frac{|C\mathbf{w}|^2}{\|\mathbf{w}\|^2} - [\lambda^R(\mathbf{w})]^2}. \quad (15)$$

Since we have chosen $\mathbf{w}^T \mathbf{w} = 1$, it is understood that in order to get the normalized eigenvector of the original GEVP, one has to apply the inverse transformation to \mathbf{w} and normalize the result, i.e.,

$$\mathbf{v} = [L^T]^{-1} \mathbf{w} / \|[L^T]^{-1} \mathbf{w}\|. \quad (16)$$

B. Algorithm implementation

The OF in Eq. (13) is explicitly written as follows:

$$f(C, \mathbf{w}, \tilde{\lambda}) = \mathbf{w}^T \mathcal{S}(\tilde{\lambda}) \mathbf{w} = \sum_{i,j} w_i w_j \mathcal{S}_{i,j}, \quad (17)$$

where \mathcal{S} is an $n \times n$ matrix (n is dictated by the discretization method applied to the hBSE) given by

$$\mathcal{S}_{i,j}(\tilde{\lambda}) = \tilde{\lambda}^2 \delta_{i,j} - \tilde{\lambda} (C_{i,j} + C_{j,i}) + \sum_{\ell} C_{\ell,i} C_{\ell,j}, \quad (18)$$

and $\mathbf{w} \equiv \{w_i\}$ is a normalized vector. By using the binary representation introduced in Appendix B, the components $w_i \in [-1, 1]$ are expressed in terms of the binary basis as follows

$$w_i = -q_{i,b} + \sum_{\ell=1}^{b-1} \frac{q_{i,\ell}}{2^\ell}, \quad (19)$$

where b is the number of bits, $q_{i,\ell} = 0, 1$ and the bit $q_{i,b}$ carries the sign, i.e., for $w_i \geq 0$ ($w_i < 0$) one assigns $q_{i,b} = 0$ ($q_{i,b} = 1$). Notice that the binary expression in Eq. (19) belongs to the interval $[-1, 1)$.

The string $\{-1, 1/2, 1/4, \dots, 1/2^{b-1}\}$ is the so-called *precision vector*, \mathbf{p} , since the last term $1/2^{b-1}$ controls the precision at which $w_i \in [-1, 1)$ is approximated. Within our notation \mathbf{p} is a column vector with dimension b . Using the precision vector \mathbf{p} , it is possible to construct a rectangular matrix, P^T , with n rows and $n \times b$ columns, that allows to transform a real vector \mathbf{w} into its binary expression, and eventually $f(C, \mathbf{w}, \tilde{\lambda})$ in a form suitable for a QUBO evaluation by using a QA. In a compact form, one writes

$$\mathbf{w} = P^T \mathbf{x}, \quad (20)$$

where

$$P^T = \begin{pmatrix} \mathbf{p}^T & 0 & \dots & 0 \\ 0 & \mathbf{p}^T & \dots & 0 \\ \vdots & \vdots & \ddots & 0 \\ 0 & 0 & \dots & \mathbf{p}^T \end{pmatrix}, \quad (21)$$

and

$$\mathbf{x} = \begin{pmatrix} \mathbf{q}_{1;b} \\ \mathbf{q}_{2;b} \\ \vdots \\ \mathbf{q}_{n;b} \end{pmatrix}, \quad (22)$$

with $\mathbf{q}_{i;b} \equiv \{q_{i,1}, q_{i,2}, \dots, q_{i,b}\}$. Inserting Eq. (20) in Eq. (17) one obtains (see Appendix B for details)

$$f(C, \mathbf{w}, \tilde{\lambda}) = \mathbf{x}^T PS(\tilde{\lambda})P^T \mathbf{x}. \quad (23)$$

One easily recognizes that \mathbf{x} is a column vector containing $n \times b$ bits, leading to the expected QUBO form of our problem, and $PS(\tilde{\lambda})P^T$ is a square symmetric matrix, with dimensions $(n \times b) \times (n \times b)$.

Starting with some given real value of $\tilde{\lambda}$ (see the next subsection), that guides the algorithm toward a real-valued eigenpair, the SA or the QA returns a binary vector \mathbf{x} for each annealing cycle N_A . Among the N_A vectors \mathbf{x} we select the one that gives the minimal value of $f(C, \mathbf{w}, \tilde{\lambda})$. Such a vector allows to get \mathbf{w} , necessary for calculating $\lambda^R(\mathbf{w})$ and $\lambda^I(\mathbf{w})$, using Eqs. (14) and (15), respectively. To accurately determine \mathbf{w} , which minimizes at the same time the number of bits required in the QA, a two-step search is implemented: the first step is the guess phase (GP), and the second one is the iterative gradient-descent phase (DP) (see, e.g., Refs. [28–30] for the symmetric case).

C. Initial guess for the nonsymmetric case

Differently from what happens for the symmetric case [28–30,32], the nonsymmetric one leads to a nonlinear dependence on the scalar parameter $\tilde{\lambda}$, and therefore the search needs a particular care. It should be emphasized that the OF is minimized by the *entire* set of real eigenpairs. Hence, in order to point to the largest, positive real eigenvalue, we need to add further information to our algorithm. We can guide the search of the minimum by using the Gershgorin circle theorem (see, e.g., Ref. [58,59], for an introduction). Noteworthy, it provides bounds for each eigenvalue of a given complex matrix, allowing the search range to be narrowed.

The theorem yields

$$|\lambda - a_{ii}| = \sum_{j \neq i} \left| \frac{a_{ij}x_j(\lambda)}{x_i(\lambda)} \right| \leq \sum_{j \neq i} |a_{ij}| = R_G(a_{ii}), \quad (24)$$

where λ is an eigenvalue of the given matrix, with elements a_{ij} , and $x_{i(j)}(\lambda)$ are components of the corresponding eigenvector, such that $|x_j/x_i| \leq 1$, $\forall j \neq i$. Hence, an eigenvalue belongs to a proper disc, with radius $R_G(a_{ii})$ and center a_{ii} . The same is valid by summing over the columns, once the transpose is considered. It is also worth mentioning a second Gershgorin theorem [59]. It proves that if a disc is disconnected from all the others, then it contains one and only one eigenvalue, which necessarily is real (the complex ones are conjugated).

Inspired by the Gershgorin theorem, a suitable permutation can be applied in order to rearrange the matrix C in Eq. (11), so that the diagonal elements are in decreasing order, i.e., $c_{11} \geq c_{22} \geq \dots \geq c_{(n \times b)(n \times b)}$. The initial value of $\tilde{\lambda}$ is chosen equal to c_{11} . The matrix $PS(\tilde{\lambda})P^T$ is passed to the QA or the SA. For each of the N_A^{GP} annealing cycles the binary vectors \mathbf{x}_α , and the corresponding values of the OF is returned. With α we label the annealing cycle. Following the Gershgorin constraint, we analyze the set

$$\{\mathbf{x}_\alpha, f(C, \mathbf{w}_\alpha, \tilde{\lambda} = c_{11}), \lambda^R(\mathbf{w}_\alpha), \lambda^I(\mathbf{w}_\alpha)\},$$

and eliminate the solutions such that

$$|\lambda^R(\mathbf{w}_\alpha) - c_{11}| > R_G(c_{11}).$$

Among the surviving solutions, the one that satisfies the condition

$$f_{\text{best}}^{GP} = \min_{\mathbf{w}_\alpha} f(C, \mathbf{w}_\alpha, \tilde{\lambda} = \lambda^R(\mathbf{w}_\alpha)) \quad (25)$$

is retained, and $\lambda^R(\mathbf{w}_\alpha)$ is calculated. The minimization search is repeated three times, $i = 1, 2, 3$, testing if the condition $f_{\text{best};i}^{GP} < f_{\text{best};i-1}^{GP}$ is satisfied. If there is an improvement, the next run receives $\tilde{\lambda} = \lambda^R(\mathbf{w}_{\alpha_{\text{best};i}})$, otherwise the iteration stops and the GP is closed. Empirically, we found this procedure is more effective in finding a good initial eigenvector than just increasing the number of annealing samples in a single iteration. After completing the minimization search, the best pair, i.e., $\lambda^R(\mathbf{w}_{GP})$ and the corresponding real vector \mathbf{w}_{GP} , that satisfies the condition in Eq. (25), is passed to the gradient-descent phase. The algorithm of the GP is schematically illustrated in Table I, and the numerical results that illustrate the behavior of the algorithm are discussed in Sec. IV A.

D. Gradient-descent phase

The algorithm proceeds through a second phase: the gradient-descent phase, which is based on the Hessian of

TABLE I. The guess-phase search of the minimum for the OF in Eq. (17), obtained from Eq. (3) after applying a classical LDL^T factorization. An assigned number of bits b is used for the transformation to the QUBO form, Eq. (23) (see text).

 Algorithm for the guess-phase, with a given number of bits b

- 1: **Assign** the input value $\tilde{\lambda} = c_{11}$, suggested by the Gershgorin theorem
 - 2: **While** $f_{\text{best};i}^{GP} < f_{\text{best};i-1}^{GP}$, for $i = 1, 2, 3$
 - 3: Minimize the QUBO form, Eq. (23), with N_A^{GP} annealing cycles
 - 4: Look for acceptable $\lambda^R(\mathbf{w}_{\alpha_i})$ falling in the Gershgorin disc
 - 5: Among the acceptable solutions, check if $f_{\text{best};i}^{GP} < f_{\text{best};i-1}^{GP}$ and continue the loop, replacing $\tilde{\lambda}$ by $\lambda^R(\mathbf{w}_{\alpha_{\text{best};i}})$
 - 6: Put $\lambda^R(\mathbf{w}_{GP}) = \lambda^R(\mathbf{w}_{\alpha_{\text{best};i}})$ and $\mathbf{w}_{GP} = \mathbf{w}_{\alpha_{\text{best};i}}$ and pass those quantity to the gradient-descent phase
-

the OF in Eq. (17). Let us call $\boldsymbol{\delta}(z) \equiv \{\delta_i(z)\}$ the variation of the vector \mathbf{w}^z , i.e., $\boldsymbol{\delta}(z) = \mathbf{w}^z - \mathbf{w}^{z-1}$, where z labels the iterations or zoom steps of the gradient-descent phase. Note that $\mathbf{w}^0 = \mathbf{w}_{GP}$. Then, the following binary expression for the $\boldsymbol{\delta}(z)$ components holds

$$\delta_i(z) = \frac{1}{2^z} \left(-q_{i,b} + \sum_{\ell=1}^{b-1} \frac{q_{\ell,b}}{2^\ell} \right) = \frac{1}{2^z} \mathbf{p}^T \cdot \mathbf{q}_{i,b}, \quad (26)$$

where the prefactor $1/2^z$ decreases at each iteration by increasing z (cf. Refs. [28–30]). The prefactor $1/2^z$ allows to control the refinement of our search, increasing the precision of the gradient-descent method. It should be pointed out that by increasing the number of iterations, i.e., zoom steps, one could decrease the initial number of bits b in the expansion of the real vectors involved in the minimization, without worsening the accuracy of the algorithm (see also Refs. [28,29] for the symmetric GEVP).

By expanding $f(C, \mathbf{w}^z, \tilde{\lambda})$ around \mathbf{w}^{z-1} up to the second order, one gets [cf. Eqs. (17) and (18)]

$$\Delta f(C, \mathbf{w}^z, \tilde{\lambda}) = 2\boldsymbol{\delta}^T(z) \mathcal{S}(\tilde{\lambda}) \mathbf{w}^{z-1} + \boldsymbol{\delta}^T(z) \mathcal{S}(\tilde{\lambda}) \boldsymbol{\delta}(z). \quad (27)$$

The term linear in $\boldsymbol{\delta}(z)$ can be recast in a QUBO form by (i) recalling that $q_\ell = q_\ell^2$, being $q_\ell = 0, 1$, and (ii) transforming the vector $\mathcal{S}(\tilde{\lambda}) \mathbf{w}^{z-1}$ in a $(n \times b) \times (n \times b)$ diagonal matrix, where the vector components are the diagonal elements (see Ref. [28]). Then, the OF suitable for the gradient-descent phase is obtained. Specifically, recalling that one can divide or multiply by a constant an OF without affecting the minimization procedure, one has

$$\hat{f}(C, \boldsymbol{\delta}(z), \tilde{\lambda}) = \boldsymbol{\delta}^T(z) \mathcal{Q}(z, \tilde{\lambda}) \boldsymbol{\delta}(z) \quad (28)$$

where the square matrix \mathcal{Q} is given by

$$[\mathcal{Q}(z, \tilde{\lambda})]_{ij} = 2\delta_{ij} [\mathcal{S}(\tilde{\lambda}) \mathbf{w}^{z-1}]_i + \mathcal{S}(\tilde{\lambda})_{ij}, \quad (29)$$

with the elements of the symmetric matrix $\mathcal{S}(\tilde{\lambda})$ written in Eq. (18). The transformation to the binary expression of the vectors $\boldsymbol{\delta}(z)$ follows the rule given in Eq. (20).

The gradient-descent phase proceeds through iteration on z , with $z = 1, \dots, N_z$, and aims to minimize the OF in Eq. (28), starting with the value of $\tilde{\lambda} = \lambda^R(\mathbf{w}_{GP})$ and the corresponding vector \mathbf{w}_{GP} . At each zoom step z , an inner loop (labeled with i) is opened. Within this loop, the QA, or the SA, returns an ensemble of $\alpha_i = 1, 2, \dots, N_A^{DP}$ qubits states, from which we select the one with minimal energy, i.e.,

$$\hat{f}_{\text{best};i}^{DP}(z) = \min_{\boldsymbol{\delta}_{\alpha_i}(z)} \hat{f}(C, \boldsymbol{\delta}_{\alpha_i}(z), \tilde{\lambda} = \lambda^R(\mathbf{w}_{\alpha_i}^z)), \quad (30)$$

where i is the inner-loop index for a fixed z and $\mathbf{w}_{\alpha_i}^z = \boldsymbol{\delta}_{\alpha_i}(z) + \mathbf{w}_{\text{best};i-1}^z$. For the value $\alpha_i = \alpha_{\text{best}}$ in correspondence of $\hat{f}_{\text{best};i}^{DP}(z)$, we calculate the values $\lambda^{R(I)}(\mathbf{w}_{\alpha_{\text{best}}}^z; i)$, that is input for the next iteration starting with the new eigenvector $\mathbf{w}_{\text{best};i}^z = \mathbf{w}_{\alpha_{\text{best};i}}^z$. When, for a fixed z , the condition $\hat{f}_{\text{best};i+1}^{DP}(z) \geq \hat{f}_{\text{best};i}^{DP}(z)$ is found, then the internal loop on i is terminated and the value of z updated, namely $z \rightarrow z + 1$. The final best result obtained for a given z is used as starting point in the $z + 1$ iteration. The procedure is repeated until the desired precision is reached (z^{max}).

Finally, one obtains the eigenvector of the GEVP in Eq. (1) by inverting the relation in Eq. (12), i.e.,

$$\mathbf{v}_{\text{best}} = [L^T]^{-1} \mathbf{w}_{\text{best}}^{z_{\text{max}}} / \|[L^T]^{-1} \mathbf{w}_{\text{best}}^{z_{\text{max}}}\|, \quad (31)$$

where z_{max} indicates the final run of the iterative gradient-descent method and $\mathbf{w}_{\text{best}}^{z_{\text{max}}}$ is the eigenvector corresponding to the final eigenvalue

$$\lambda_{\text{best}} = \lambda^R(\mathbf{w}_{\text{best}}^z). \quad (32)$$

It should be recalled that the Hessian is always positive, so that a minimization path is ensured. The gradient-descent algorithm is sketched in Table II.

By repeating the entire minimization procedures, i.e., guess plus gradient-descent phases, given the non-deterministic nature of the annealing process, errors and fluctuations of the final results, $\{\lambda_{\text{best}}, \mathbf{v}_{\text{best}}\}$, are generated. In order to study such uncertainties, the entire algorithm was run by N_{run} times, keeping fixed the initial matrices A

TABLE II. The gradient-descent phase search of the global minimum on both SA and QA. The gradient-descent phase is based on the Hessian of the OF in Eq. (3) (see text). The same guess-phase number of bits b is used.

Algorithm for the gradient-descent phase

- 1: **Use** $\tilde{\lambda} = \lambda^R(\mathbf{w}_{GP})$, from the guess phase
 - 2: **While** $1/2^z \geq \epsilon'$ ($z \geq 1$)
 - 3: Transform the obj. function in Eq. (28) to QUBO form with $1/2^z$ in \mathbf{p}
 - 4: **While** $\hat{f}_{\text{best};z}^{DP}(i) < \hat{f}_{\text{best};z}^{DP}(i-1)$ for $i = 1, 2, 3, \dots$
 - 5: Minimize the QUBO form in Eq. (28), with N_A^{DP} annealing cycles
 - 6: Search the minimal value among the N_A^{DP} energies returned by the annealer (α_{best})
 - 7: Replace $\tilde{\lambda}$ with $\lambda_z^R(\mathbf{w}_{\alpha_{\text{best}}}; i)$
 - 8: Pass to $z + 1$ with $\tilde{\lambda} = \lambda_z^R(\mathbf{w}_{\alpha_{\text{best}}}; N_z)$
-

and B . This provides an estimate of the uncertainties associated to the annealing process, and how these uncertainties propagate through the algorithm. We performed this statistical analysis using both the noisy annealer simulator, provided by D-Wave Systems software-package, with large N_{run} , and the QA with a substantially smaller N_{run} , given the limitation on running-time at our disposal. In what follows, the results obtained with the simulator are indicated by inserting SA at the beginning of the figure captions, while the results obtained with the D-Wave *Advantage System 4.1* are labeled by QA.

IV. RESULTS

In order to study the reliability of the algorithm, we used the matrices A and B obtained from the discretization of the hBSE describing a system of two massive scalars, with mass equal to m and strong binding energy $E_B/m = 1.0$. They interact through the ladder-exchange of a massive scalar, with mass $\mu/m = 0.15$ [see Eq. (A4) in Appendix A, and for more details Ref. [38]]. In our investigation we classically evaluate the LDL^T factorization, exploiting the nonsingularity of the symmetric matrix B , and then we solve the standard eigenvalue problem given in Eq. (13). We leave to future works the generalized case. Let us recall that we focus only on the search of the largest real eigenpair. It should be recalled that, in our approach, the largest real eigenvalue corresponds to the lowest coupling constant, which is able to bind the two massive scalars. Finally, we give a first insight on the scalability of the proposed algorithm by considering matrix dimensions $n_M = 4, 8, 12, 16, 24, 32$.

In an effort to better optimize the available quantum-computing resources, a challenging issue is to guide the choice of the input parameters of the proposed algorithm. They are given by: (i) the number of bits b , needed for the binary representation of the real vectors involved in the problem, and (ii) the number of annealing cycles, i.e., N_A^{GP} , for the guess phase, and N_A^{DP} , for the gradient-descent one. This important optimization task, which is time consuming, was carried out by using the SA, and the corresponding results are discussed in the first part of this section. In the

second part, we illustrate the outcomes obtained by using the QA.

In particular, to perform the SA analysis, a matrix with dimension $n_M = 32$ was adopted and the entire algorithm was run for $N_{\text{run}} = 500$ times, in order to gather enough statistics and determine a reasonable set of input parameters to be used with the QA. For the remaining part of this work, the following symbols are adopted: (i) $\bar{\lambda}_{\text{best}}(\bar{\lambda}_{\text{best}}^I)$ is the average of $\lambda^R(\lambda^I)$ obtained from Eq. (14) [Eq. (15)] over the N_{run} runs of the algorithm for z^{max} ; (ii) $\|\mathbf{v}_{\text{true}} - \mathbf{v}_{\text{best}}\|$ indicates the mean Euclidean distance, where \mathbf{v}_{true} is the real eigenvector of the original GEVP, and \mathbf{v}_{best} computed for z^{max} is given in Eq. (31).

A. Running the guess-phase on the SA

Selecting a reliable initial guess in the first phase of the algorithm, sketched in Table I, is a crucial step for obtaining an accurate result in the subsequent gradient-descent phase. As already mentioned, all the real-valued eigenpairs are acceptable for the annealer, and therefore one has to guide the search toward the target solution, i.e., the real eigenpair with the largest real eigenvalue. In addition, one has to carefully consider another source of numerical challenges: the (necessarily) finite number of bits b . In fact, one has to assign b for representing the components of the normalized vector entering the definition of the QUBO OF in Eq. (23), and eventually construct the matrix PSP^T . This obvious limitation can generate *spurious* minima, and direct the path toward a wrong target. An example is shown in Fig. 1, where the case of the three largest real eigenvalues, $\lambda_1 > \lambda_2 > \lambda_3$, is studied. For bit numbers $b = 3, 4, 6, 8$ and running the entire algorithm only one time (i.e., $N_{\text{run}} = 1$), the values of $\lambda^R(\mathbf{w}_\alpha)$, Eq. (14), obtained in the guess-phase from each of the $N_A^{GP} = 2000$ annealing cycles on the SA, are plotted as a function of the corresponding annealer energies divided by $[\lambda^R]^2$ (this is suggested by the quadratic dependence of the OF on $\tilde{\lambda}$ and the purpose of assigning a normalization to different outcomes). Notice that the annealer energies correspond to the values of Eq. (23) as returned by the annealer in the QUBO form i.e., with the binary vectors not normalized.

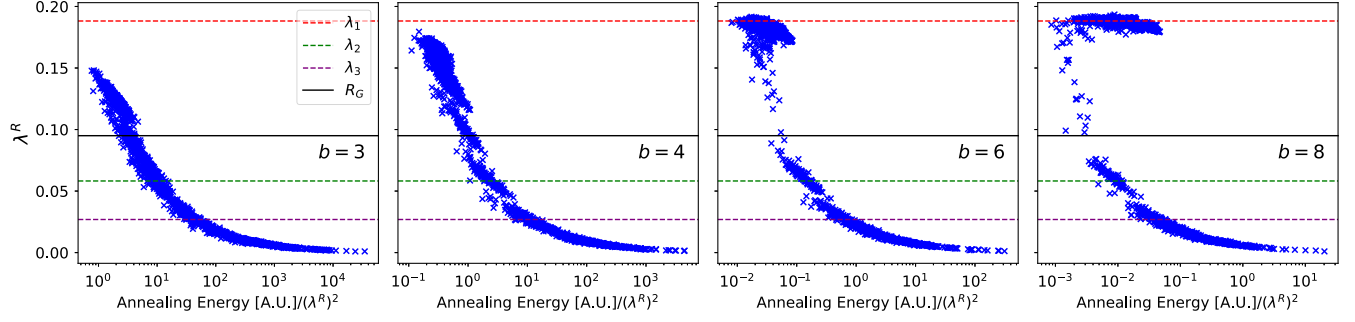


FIG. 1. SA: scatter plot of the $N_A^{GP} = 2000$ guess-phase values λ_a^R , Eq. (14), vs the corresponding annealer energies divided by $[\lambda^R]^2$, for the bit numbers $b = 3, 4, 6, 8$ used to get the QUBO matrix $PSPT$, Eq. (23), with dimension $32 \times b$. Dashed lines: the three largest real eigenvalues, $\lambda_1 > \lambda_2 > \lambda_3$ of the matrix C , Eq. (11). Solid line: $|c_{11} - R_G(c_{11})|$ with $R_G(c_{11}) = \sum_{j \neq 1} |c_{1j}|$, i.e., the lower limit of the Gershgorin disc, with center $c_{11} = 0.190$.

In Fig. 1, the dashed horizontal lines represent the three largest real eigenvalues (calculated classically) of the 32×32 matrix C in Eq. (11). The solid line is the lower extremum of the Gershgorin disc, with center $c_{11} = 0.190$. Such an extremum is the lowest value admissible for λ_1 . In the various panels, one observes several regions where the results appear to clusterize despite the initial guess $\tilde{\lambda} = c_{11}$ is very close to the actual eigenvalue $\lambda_1 = 0.188225$. Once a more detailed analysis is performed, it can be shown that the clusterization is present already at $b = 3$, although it is not observable in the figure. Moreover, some clusters approach the minima generated by the other two eigenpairs, with eigenvalues λ_2 and λ_3 , while others are *spurious* minima, that are generated by the limited precision of the assigned binary representation, i.e., 3 bits. By increasing b , the clusters migrate close to the actual eigenvalues, with smaller and smaller energies (notice the different x -axis scale for the four panels). At the same time, a larger amount of points are approaching λ_1 , given the increasing precision, although they spread over a wider range of energy as expected. This is due to the increase of states degeneration when the number of b increases, since the returned bit strings are neither normalized nor orthogonal.

Interestingly, λ_1 is approached from below by increasing b . This behavior can be understood considering the bias due to the spectrum of the matrix under scrutiny. In fact, the decreasing ordering of the real eigenvalues, that follows from the chosen ordering of the matrix elements along the main diagonal, can generate the observed pattern, since the annealing process should clearly spend a non-negligible amount of time to explore the minima corresponding to the part of the spectrum below λ_1 . It turns out that the feature persists, even after running many times the code.

Increasing b allows to refine the solution found by the annealer. On the other hand, a larger value of b implies a larger dimension of the matrix representing the OF. Unfortunately, such matrix dimension is constrained by the actual topology of the qubits network during the process of minor-embedding (see below). This limits the precision of

our solution in the initial guess phase. Fortunately, as also discussed in Refs. [28,29], a reasonable compromise can be reached by properly increasing the number of iterated annealing cycles and adopting a small number of bits, as investigated in the following gradient-descent phase.

In order to gain insights on the mapping of the OF in Eq. (13) and the one given in terms of the binary strings, it is useful to show an analysis equivalent to the one in Fig. 1, but focusing on the values of the OF in Eq. (13), where normalized vectors are used. In particular, the cases with $b = 3$ and $b = 8$ are shown in Fig. 2, where the squares are the solutions selected after applying the Gershgorin criterium with $R_G(c_{11})$. The clusterization is more evident than in Fig. 1 and presents a different overall behavior compared to the results directly obtained from the annealing process. In particular, the accuracy of the OF mapping onto the binary basis improves by increasing the number of bits, and the annealer spend more and more time close to the actual minima.

Summarizing, two main consequences can be deduced from the calculations shown in Figs. 1 and 2. First, in the guess phase, it is not possible to select the final value of λ^R only on the basis of the annealer energies, as in the symmetric case (see, e.g., Refs. [28,29]), but we need the Gershgorin criterium, to overcome the issue of the quadratic dependence on $\tilde{\lambda}$ in the OF. Second, we note that by exploiting the mentioned quadratic dependence, the annealer becomes a powerful tool to explore a wide portion of the spectrum of our eigenvalue problem. In principle, it is possible to identify also the other eigenpairs, by studying the clusterization of the returned energies. This appealing feature will be investigated elsewhere.

In Fig. 3, the GP success-rate, i.e., the number of times the algorithm is able to find a solution falling inside the Gershgorin disc, is shown as a function of the GP annealing cycles, N_A^{GP} , for $b = 3$ and running the code $N_{run} = 500$ times for the 32×32 matrix. A number of ~ 200 annealing cycles seems to guarantee a 100% probability of having at least one point within the Gershgorin disc, by using the SA.

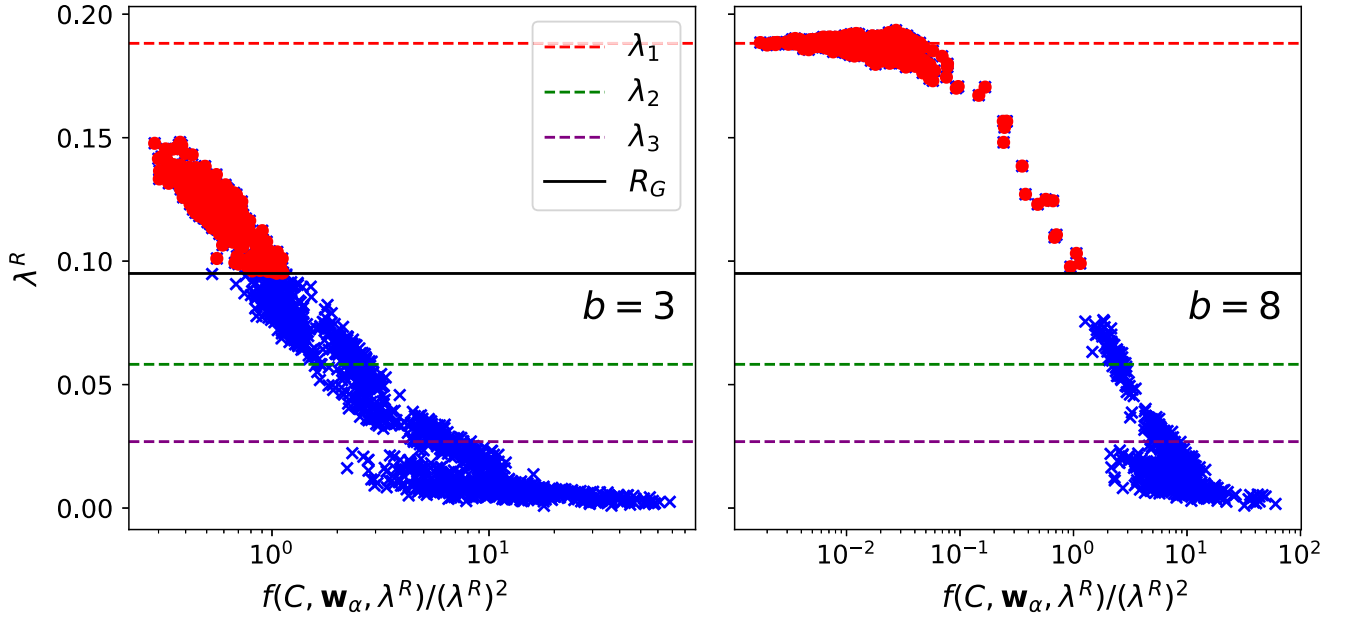


FIG. 2. SA: the same as the panels $b = 3$ and $b = 8$, in Fig. 1, but with the values of $f(C, \mathbf{w}_\alpha, \lambda^R)/(\lambda^R)^2$, Eq. (13), on the x -axis, instead of the annealing energies [see Eq. (23)]. Recall that here the vector \mathbf{w}_α is normalized. Red squares are the solutions selected after applying the $R_G(c_{11})$ cut, and blue crosses are the solutions outside the Gershgorin disc.

Since it is crucial to receive as reliable input as possible from the guess phase, so that a better final outcome could be reached, we attempted to find a tighter bound, if any, for $\tilde{\lambda}$ to be used in the initial run of the gradient-descent phase. In order to implement this, we arbitrarily reduced the Gershgorin radius, $R_G(c_{11})$, to a chosen value r . In Fig. 4, the GP success-rate for the above 32×32 matrix is analyzed by (i) taking $b = 3$ and (ii) running $N_{\text{run}} = 500$ times the GP algorithm with annealing cycles $N_A^{GP} = 200$. As expected, the GP success-rate decreases

by reducing r , and we were not able to find any solution below $r/R_G < 0.4$. In conclusion, for the matrices considered in this work, the most reasonable and practical choice is $r = R_G(c_{11})$.

B. Running the gradient-descent phase on the SA

The main goal of the gradient-descent phase is the improvement of the accuracy in determining the searched

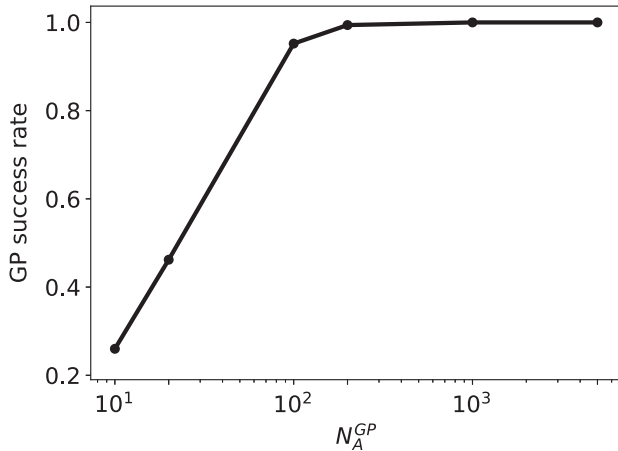


FIG. 3. SA: guess-phase success-rate vs N_A^{GP} , for a 32×32 matrix in Eq. (13). The solid line was obtained considering $N_{\text{run}} = 500$ independent samples with $b = 3$ (see Table I for the outline of the algorithm in the guess-phase).

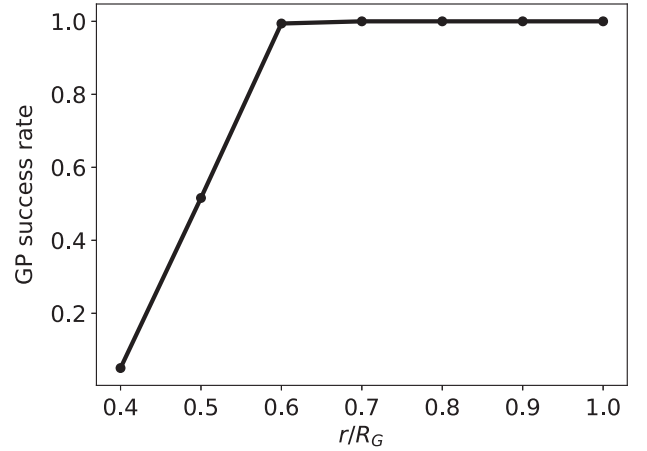


FIG. 4. [SA] Guess-phase success-rate vs an arbitrary reduction of the Gershgorin radius (represented by the ratio r/R_G), for a 32×32 matrix in Eq. (13). The solid line was obtained by considering $N_{\text{run}} = 500$ independent samples, with $b = 3$ and $N_A^{GP} = 200$ (see Table I for the outline of the algorithm in the guess phase).

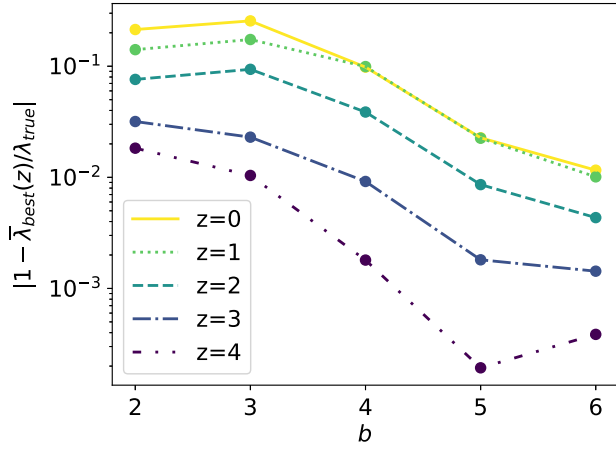


FIG. 5. SA: relative precision $|1 - \bar{\lambda}_{\text{best}}(z)/\lambda_{\text{true}}|$, at fixed zoom step, vs the number of bits b . In the calculations, we used $N_A^{GP} = 200$, $N_A^{DP} = 20$. The dots represent the mean of the relative precision obtained from $N_{\text{run}} = 500$ independent samples.

eigenpair. We pursued this scope by decreasing the prefactor $1/2^z$, with $z \geq 1$, in Eq. (26). In this subsection we focus on the impact of the input parameters by increasing this prefactor. Notice that for all the analysis carried out in this section, we run $N_{\text{run}} = 500$ independent simulations.

In Fig. 5, the relative precision $|1 - \bar{\lambda}_{\text{best}}(z)/\lambda_{\text{true}}|$ [cf. Eq. (32)] dependence on the number of bits, $b \geq 2$, is presented for various zoom steps z (in what follows, $z = 0$ indicates the guess phase and the values $z \geq 1$ belong to the gradient-descent phase). The dots in the figure are the mean, over 500 independent runs, of the relative precision obtained by using $N_A^{GP} = 200$, and $N_A^{DP} = 20$. An overall decreasing pattern can be observed for increasing b and fixed z , that can be largely ascribed to a better identification of the minimum during the guess phase, $z = 0$ (see Sec. IV A). Interestingly, the numerical outcomes shown in Fig. 5 suggest that it is possible to establish a fair trade-off between the number of bits and the number of zoom steps in order to achieve increasingly accurate results, as already observed for the symmetric GEVP (see, e.g., Refs. [28,29]). One should recall that the lower the number of bits, the lower the dimension of the QUBO matrix, and thus the less difficult the eigenpair search becomes.

In Fig. 6, the relative precision at fixed zoom step was studied by changing the number of annealing cycles during the gradient-descent phase, N_A^{DP} , keeping fixed $N_A^{GP} = 200$ and $b = 3$. The figure shows that there is basically no improvement by increasing N_A^{DP} . In the gradient-descent phase for a given z , the algorithm requires a minimal number of annealing cycles to find the best minima for $\delta(z)$. This is one of the advantage of using such an algorithm.

In conclusion, the campaign of numerical calculations performed on the SA has suggested to adopt the following

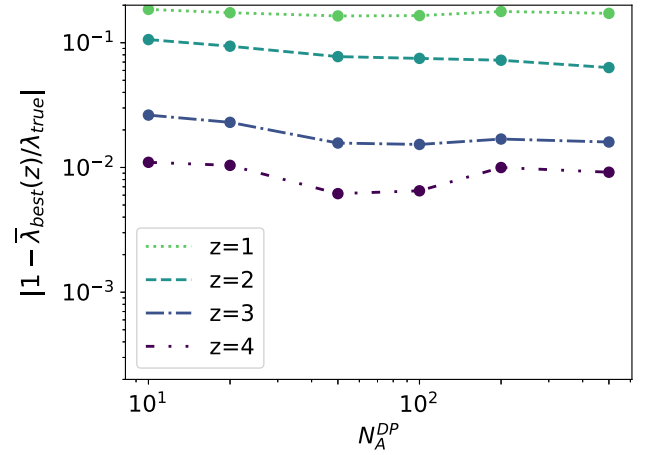


FIG. 6. SA: the relative precision $|1 - \bar{\lambda}_{\text{best}}(z)/\lambda_{\text{true}}|$, at fixed zoom step, vs N_A^{DP} , the number of annealing cycles in the gradient-descent phase. In the calculations, $N_A^{GP} = 200$ and $b = 3$ were used. The dots represent the mean of the relative precision performed over $N_{\text{run}} = 500$.

input parameters for the studies of our algorithm on the QA: $N_A^{GP} = 200$, $N_A^{DP} = 20$, and $b = 2$ or $b = 3$, but with a suitable number of zoom steps. This preliminary analysis is critical to fine-tune the strategy when the QA comes into play and a limited run-time is available. It also sheds light on the different behavior of QA and SA, with obvious practical implications for the analysis of large matrices.

C. Analysis of the QA results

We perform the *experimental* study of the algorithm by using the *Advantage 4.1* quantum annealer, provided by D-Wave Systems. As a first step, we adopted $N_A^{GP} = 200$ and $N_A^{DP} = 20$ in order to study the whole set of matrices whose relevant eigenpairs we aim to determine. As for the number of bits, we used $b = 3$ for $n_M < 16$ and $b = 2$ for $n_M \geq 16$, in order to avoid limitations on the matrix dimensions that can be processed by the QA. In fact, the current QA has a given upper-bound on the number of logical qubits to be mapped onto sets of physical qubits, organized with an assigned topology.²

In Table III we show the summary of the QA results for the problem in Eq. (1), with dimensions $n_M = 4, 8, 12, 16, 24, 32$. As target we selected a nominal relative precision on the eigenvalue of $\epsilon' = 10^{-3}$ that in the algorithm corresponded to a value of $z = 9$.

²This process is called minor-embedding or simply embedding. Recall that the matrix dimension in the QUBO problem is $n_M \times b$, and therefore $n_M \times b$ logical qubits are fully connected with weights given by the values of the matrix elements. For the *Advantage 4.1* system [26,27], based on the Pegasus topology of the physical qubits, a maximal size of a fully connected set of logical qubits (clique) is 177, but it can be reached under very peculiar conditions, not fully achievable in our actual problem, if accurate results have to be obtained.

TABLE III. QA: results obtained by using the *Advantage 4.1* quantum annealer, provided by D-Wave Systems. In the table, n_M is the dimension of the matrices A , B and C involved in the calculations [see Eqs. (1) and (11), respectively]; b is the number of bits adopted for the matrix representation in the QUBO problem [see Eq. (23)]; N_{run} is the number of runs of the entire algorithm (guess phase + gradient-descent phase); $\bar{\lambda}_{\text{best}}$ is the average of $\lambda_{\text{best}}(z_{\text{fin}}) = \lambda^R(\mathbf{w}_{\alpha_{\text{fin}}})$ [cf. Eq. (14) and the definition below Eq. (31)], over the outcomes returned after running the entire algorithm N_{run} times; in $\bar{\lambda}_{\text{best}}^I/\bar{\lambda}_{\text{best}}$ the numerator $\bar{\lambda}_{\text{best}}^I$ is obtained as $\bar{\lambda}_{\text{best}}$, but following Eq. (15); $\|\mathbf{v}_{\text{true}} - \mathbf{v}_{\text{best}}\|$ is the mean Euclidean distance between the true eigenvector and the one from the QA (recall that the vectors \mathbf{v}_i are normalized). In addition to the mean values, the 68% confidence interval is shown. All the results are obtained using $z = 9$ zoom steps, corresponding to an upper bound for the relative precision equal to $\epsilon' = 10^{-3}$.

n_M	b	N_{run}	λ_{true}	$\bar{\lambda}_{\text{best}}$	$\bar{\lambda}_{\text{best}}^I/\bar{\lambda}_{\text{best}}$	$\ \mathbf{v}_{\text{true}} - \mathbf{v}_{\text{best}}\ $
4	3	80	0.188026	$0.188012^{+1 \times 10^{-5}}_{-7 \times 10^{-6}}$	$0.00024^{+2 \times 10^{-5}}_{-5 \times 10^{-6}}$	$0.00024^{+3 \times 10^{-5}}_{-2 \times 10^{-5}}$
8	3	80	0.188204	$0.18820^{+2 \times 10^{-5}}_{-2 \times 10^{-5}}$	$0.0003^{+1 \times 10^{-4}}_{-1 \times 10^{-4}}$	$0.0003^{+1 \times 10^{-4}}_{-1 \times 10^{-4}}$
12	3	80	0.188203	$0.18821^{+2 \times 10^{-5}}_{-2 \times 10^{-5}}$	$0.0005^{+1 \times 10^{-4}}_{-1 \times 10^{-4}}$	$0.0006^{+2 \times 10^{-4}}_{-1 \times 10^{-4}}$
16	2	80	0.188203	$0.18820^{+4 \times 10^{-5}}_{-3 \times 10^{-5}}$	$0.0009^{+1 \times 10^{-4}}_{-1 \times 10^{-4}}$	$0.0011^{+2 \times 10^{-4}}_{-2 \times 10^{-4}}$
24	2	80	0.188225	$0.18822^{+5 \times 10^{-5}}_{-4 \times 10^{-5}}$	$0.0013^{+1 \times 10^{-4}}_{-3 \times 10^{-4}}$	$0.0015^{+3 \times 10^{-4}}_{-2 \times 10^{-4}}$
32	2	200	0.188225	$0.18823^{+4 \times 10^{-5}}_{-3 \times 10^{-5}}$	$0.0016^{+2 \times 10^{-4}}_{-2 \times 10^{-4}}$	$0.0018^{+4 \times 10^{-4}}_{-3 \times 10^{-4}}$

In the fifth column, we present the mean value $\bar{\lambda}_{\text{best}}$ obtained running the algorithm N_{run} times. The agreement between the *true* eigenvalue, λ_{true} in the fourth column, and the mean value $\bar{\lambda}_{\text{best}}$ is smaller than the nominal precision requested $\epsilon' = 10^{-3}$. More importantly, all the results obtained in our runs are better than the requested precision. This can be observed by comparing the 68% confidence interval over the N_{run} runs with the nominal precision $\epsilon' = 10^{-3}$.

In Table III we also show: (i) the ratio $\bar{\lambda}_{\text{best}}^I/\bar{\lambda}_{\text{best}}$, and (ii) the mean Euclidean distance $\|\mathbf{v}_{\text{true}} - \mathbf{v}_{\text{best}}\|$. It is worth noting that the ratio and the mean Euclidean distance have almost the same magnitude, and slightly increases with the matrix dimension n_M . In view of this, a remarkable degree of reliability of the proposed algorithm can be inferred.

In Fig. 7 we plot the two dimensional distribution of the results obtained running the code for $N_{\text{run}} = 200$ in the $n_M = 32$ case for $z = 6$ and $z = 9$ as function of $(1 - \lambda_{\text{best}}/\lambda_{\text{true}})$, and the Euclidean distance $\|\mathbf{v}_{\text{true}} - \mathbf{v}_{\text{best}}\|$, where λ_{best} and \mathbf{v}_{best} are the solution found by the algorithm (notice the difference with $\bar{\lambda}_{\text{best}}$). It is worth noticing that the relevant area substantially shrinks when passing from the distribution of the results for $z = 6$ to $z = 9$, as shown by the changes in the $x - y$ scales, but it is not possible to identify a direct correlation between the two quantities. However, the results seems to accumulate on a circular region that does not change shape increasing z indicating that the correlation does not depend on the specific zoom phase. We observed also that the projection on the x axis, the distribution of $(1 - \lambda_{\text{best}}/\lambda_{\text{true}})$, approaches a Gaussian distribution centered in zero with a smaller and smaller width as z increases, while the projection on the y axis, the Euclidean distance, starts from zero and extend to positive values, still with a Gaussian fall-off. Plainly, these distributions are very important for a better understanding of the

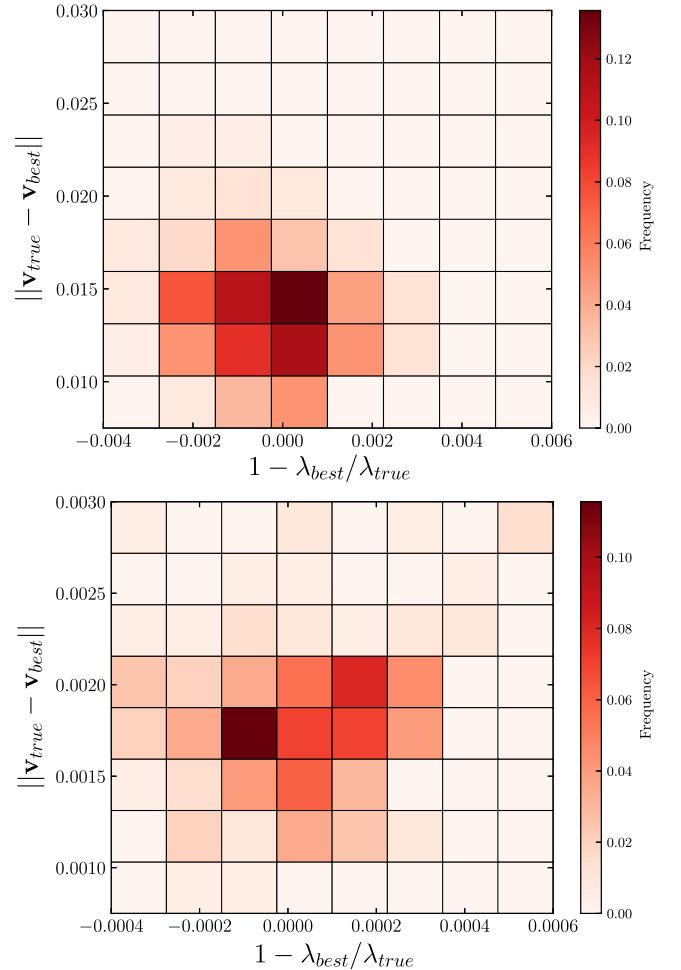


FIG. 7. QA: two dimensional distribution of the results for the $n_M = 32$ case, after running $N_{\text{run}} = 200$ times the entire algorithm as a function of the Euclidean distance $\|\mathbf{v}_{\text{true}} - \mathbf{v}_{\text{best}}\|$ vs the precision $(1 - \lambda_{\text{best}}/\lambda_{\text{true}})$. Upper panel: $z = 6$ results. Lower panel: $z = 9$ results.

quantum-hardware behavior and should be carefully investigated in a future work, when a much longer QA running-time will be available for exploring larger N_{run} and lower ϵ' .

D. Is the QA advantageous?

The algorithm presented in this paper can work in general with any kind of optimizer and it is not necessarily limited to the use of an annealer (simulated or quantum). For example, we performed some tests by running a random-sampling simulation, and got numerical results comparable to the ones obtained by using the QA, only for a matrix with dimension 4×4 . In particular, to achieve results for $n_M = 4$ and $b = 3$ similar to the ones obtained by calling the QA 200 times for the guess phase and 20 for the descent one, we sampled the space a number of times $\sim 4 \times 10^3$, with a substantial increase of the running time. For larger matrices, the number of samplings exponentially grows and in parallel the running time.

Moreover, in order to understand the differences between the classical and the quantum annealing, a comparison between the outcomes obtained for matrix dimensions $n_M = 4$ and 32 from SA and QA is provided. The results are shown in Figs. 8–11, for both the eigenvalue and the eigenvector, respectively. For matrix dimensions $n_M = 4$, the analysis has been carried out by using $b = 3$ and pushing the number of zoom step beyond $z = 30$ (recall that in the calculations shown in previous figures the maximal value is $z = 9$, leading to a nominal precision $\epsilon' = 10^{-3}$). For the case $n_M = 32$, the number of bits was reduced to $b = 2$, as already explained, and the zoom steps exceeded $z = 20$.

In Figs. 8 and 9, the mean relative precision $|1 - \bar{\lambda}_{\text{best}}(z)/\lambda_{\text{true}}|$ for fixed z is shown for $n_M = 4$ and $n_M = 32$, respectively. Red squares and arrows represent the mean and the worst result obtained over $N_{\text{run}} = 1000$ simulations, respectively. Green triangles and arrows are the same as before, but running the entire algorithm on QA by $N_{\text{run}} = 10$ times for $n_M = 4$ and by $N_{\text{run}} = 8$ times for $n_M = 32$. We reduced the number of runs used for this study compared to the one in Table III, because of the larger running-time requested to go beyond $z = 9$. Finally, blue dots are the results obtained using the exact, classical solver for the QUBO problem at each zoom step. These blue dots are not available for $n_M = 32$, since it should be necessary to poll 2^{64} states and infer the suitable distributions (i.e., the well-known Feynman's argument in favor of a quantum computer).

As clearly seen in Figs. 8 and 9, the actual accuracy improves substantially as z increases for both SA and QA. In general, it remains below the nominal precision $1/2^z$, given by the dashed lines. For $n_M = 4$, the results obtained with SA and QA are below $1/2^z$ up to $z = 25$, reaching a plateau with a rough value of $\sim 10^{-8}$. For $n_M = 32$, the SA reach a plateau roughly around $\sim 10^{-6}$ while the QA shows

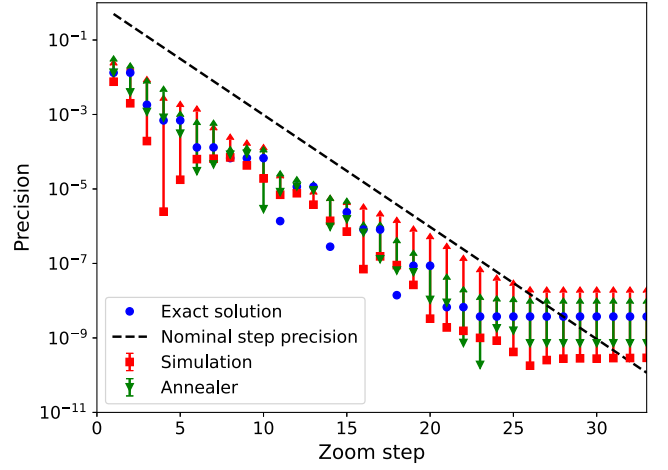


FIG. 8. SA–QA: mean relative precision, $|1 - \bar{\lambda}_{\text{best}}(z)/\lambda_{\text{true}}|$, vs the zoom step in the gradient-descent phase, for $n_M = 4$ case with $b = 3$. The dashed line is the nominal precision at each zoom step, equal to $1/2^z$. Red squares and arrows represent the mean and the worst result respectively, obtained by averaging over $N_{\text{run}} = 1000$ runs on the SA. Green triangles and arrows are the same as before obtained with the QA, but averaging over $N_{\text{run}} = 10$ runs. Blue dots are the results obtained using the exact solver for the QUBO problem at each zoom step.

a behavior close to the one seen for $n_M = 4$. From the comparison between $n_M = 4$ and $n_M = 32$ SA results, one could ascribe the different behavior to a lower SA's performance in managing large matrices, rather than an issue with the algorithm. In fact, the results obtained with the QA just follows the expected behavior. One could understand heuristically the presence of a plateau by considering that the actual zero of the OF $f(C, \mathbf{w}, \tilde{\lambda})$ is numerically about 10^{-16} , and therefore a precision for $\tilde{\lambda}$ of the order of \sqrt{f} , i.e., $\sim 10^{-8}$, is expected. Properly rewriting Eq. (13), one gets

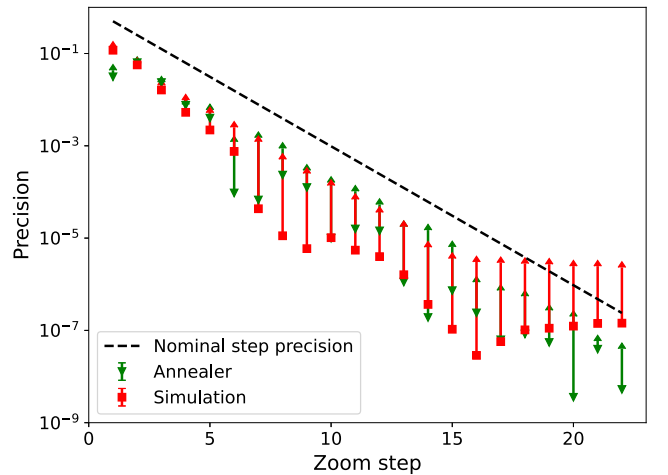


FIG. 9. SA–QA: the same as Fig. 8, but for $n_M = 32$ and $b = 2$. The QA results are obtained by averaging over $N_{\text{run}} = 8$ runs (see text).

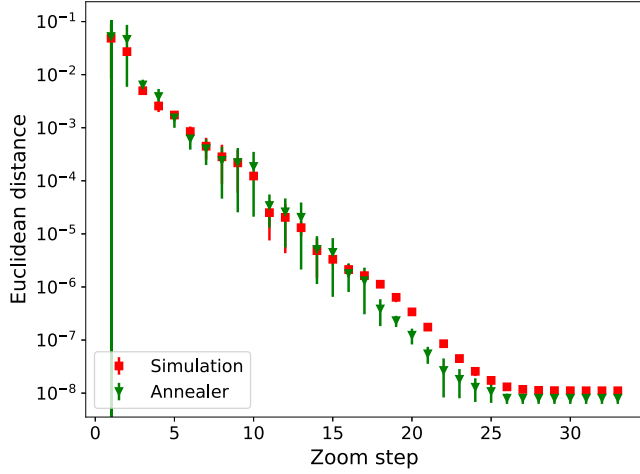


FIG. 10. SA–QA: mean Euclidean distance between the target eigenvector and the true one, at each zoom step, for the $n_M = 4$ case with $b = 3$. Green triangles: results from the QA. Red squares: outcomes from the SA. Error bars represent the 99% confidence level over 10 (1000) runs on the QA (SA).

$$\frac{f(C, \mathbf{w}, \tilde{\lambda})}{|\mathbf{w}|^2} = [\tilde{\lambda} - \lambda^R(\mathbf{w})]^2 + [\lambda^I(\mathbf{w})]^2, \quad (33)$$

that for real $\tilde{\lambda}$ leads to the above estimate.

The Euclidean distance between the target eigenvector and the results obtained, at each zoom step, with the SA and the QA, is shown in Figs. 10 and 11, for $n_M = 4$ and $n_M = 32$, respectively. The symbols are the same as in Figs. 8 and 9, while the error bars represent the 99.9% confidence level. As expected, the Euclidean distance decreases by increasing z , until it reaches a plateau following a pattern similar to the eigenvalue relative precision. Again, for $n_M = 32$, the QA performs better than the SA.

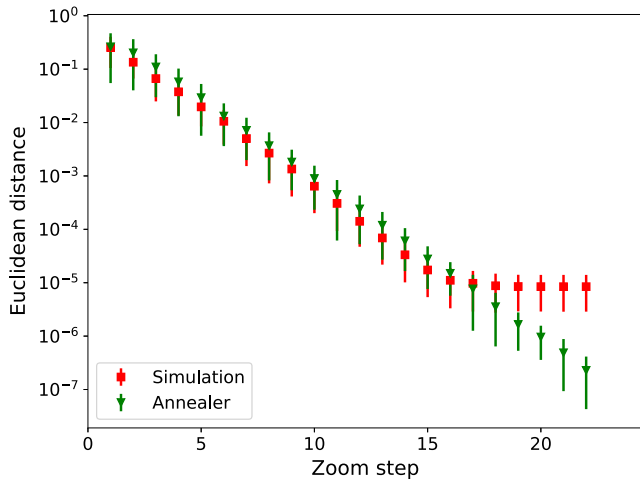


FIG. 11. SA–QA: the same as Fig. 10, but for $n_M = 32$ and $b = 2$. The QA results are averaged over $N_{\text{run}} = 8$ runs.

Summarizing, the proposed algorithm opens an actual window on the study of the spectrum of nonsymmetric matrices by using a QA. In particular, our algorithm applied to QA outperforms the random-sampling optimization method and our results suggest that it also outperforms the simulated annealing. Clearly, the algorithm is still limited to small matrices, but this will be surely overcome by the planned improvements of the QPU topology, so that larger and larger matrices will be embedded. In the present stage, our algorithm together with the QA is still limited in comparison with the classical LAPACK [60] approach. However, in the future a detailed comparison among the two algorithms is recommended, since the minimal number of matrix operation required in our algorithm (substantially only matrix vector products) suggests a good scalability with the matrix dimension.

E. Scalability on the QA

A first study of the scalability of the proposed hybrid algorithm running on the QA has been carried out by focusing on the total time spent in the annealing cycles. In our case, the total annealing-time is theoretically given by $3 \times N_A^{GP} \times t + z^{\max} \times i^{\max} \times (N_A^{DP} \times t)$ (cf. Tables I and II) where $t \sim 20 \mu\text{s}$ is the annealing time selected, z^{\max} is the maximal value of zoom steps adopted in the gradient-descent phase, e.g., for the results shown in the third column of Table III one has $z^{\max} = 9$. Moreover, i^{\max} is the maximal number of search cycles for a given z (see step 4 in Table II). In Table IV, $T[\text{ms}]$ is the total annealing-time averaged on N_{run} runs of the two-phase algorithm. One notices that a slightly increasing behavior is present when the matrix dimension, $n_M \times b$, increases, at fixed b . But, further studies with larger matrices will be necessary for fully assessing a linear increasing of the total annealing time on the QA.

Another parameter to be considered when studying the scalability of the algorithm is the number of physical qubits, N_{qubits} , used by the annealer to map the logical qubits of the QUBO problem on the topology of the hardware (Pegasus in this case), through the embedding process. This is deeply interconnected with the constraints

TABLE IV. QA: total annealing time, $T[\text{ms}]$, and total number of physical qubits N_{qubits} , averaged on N_{run} runs, for the results shown in Table III.

$n_M \times b$	N_{run}	$T[\text{ms}]$	N_{qubits}
12(4 × 3)	80	18.5 ^{+0.9} _{-0.7}	24.1 ^{+0.9} _{-1.1}
24(8 × 3)	80	21.7 ^{+1.3} _{-0.9}	81.3 ^{+2.1} _{-2.3}
32(16 × 2)	80	23.0 ^{+1.4} _{-1.0}	140.9 ^{+1.9} _{-1.9}
36(12 × 3)	80	23.0 ^{+1.4} _{-1.3}	177.6 ^{+6.4} _{-6.6}
48(24 × 2)	80	23.0 ^{+1.0} _{-1.0}	306.6 ^{+11.8} _{-15.6}
64(32 × 2)	200	23.6 ^{+1.2} _{-1.2}	529.8 ^{+30.6} _{-33.8}

posed by the quantum hardware and it is a hard problem by itself (interested readers may find useful information in Refs. [61,62], where theoretical analyses of heuristic algorithms for embedding are discussed, also in relation to the approach pursued by D-Wave). In general, since each physical qubit is not connected to all the other, the mapping is not a one-to-one correspondence, but it is a one-to-many, i.e., one logical qubit is represented by a set of physical qubits, all in principle forced to have the same value. For this formal step we rely on the algorithm elaborated by the PROPRIETARY software D-Wave Ocean, mainly based on the Cai *et al.* heuristic algorithm [63]. Since the software is heuristic, a different embedding,³ with a different number of physical qubits, is used at each QA run. However, the exact number of physical qubits adopted for mapping the QUBO square matrix is provided by the software, so that the distribution of N_{qubits} over different runs can be eventually obtained. The mean value and the 68% confidence level of the number of this distribution is then showed in the last column of Table IV. It should be noted that the number of involved physical qubits is roughly given by the matrix dimension times the so-called chain length, i.e., the number of qubits needed for representing a single logical qubit. In our analysis, the chain length linearly grows with the matrices dimension as shown in Ref. [26].⁴ The overall memory required by the algorithm grows therefore quadratically with the dimension of the original matrix.

V. CONCLUSIONS AND PERSPECTIVES

A hybrid algorithm, suitable for a quantum annealer, was implemented to evaluate the largest real eigenvalue and corresponding eigenvector of a generalized eigenvalue problem involving a nonsymmetric matrix. This numerical problem stems from the discretization of the homogeneous Bethe-Salpeter equation describing a bound state of two massive scalars, that interact by exchanging a massive scalar (see, e.g., Ref. [38]). In the current initial stage of the study, the nonsingularity of the symmetric matrix was exploited, so that a classical LDL^T factorization of the symmetric matrix was used in order to deal with a simpler QUBO problem.

The numerical results were obtained by running our two-phase algorithm both on an *Advantage 4.1* quantum

annealer, provided by the D-Wave Systems, and a simulator, based on the PROPRIETARY software Ocean. We first tested our algorithm, based on an OF suggested in Ref. [39] and supplemented by the result of the valuable Gershgorin circle theorem [59], on the SA. This first investigation led to establish a practical set of input parameters, given by: (i) the number of bits for expressing the real components of the involved vectors in the binary basis, and (ii) the number of annealing cycles in both the guess phase and the gradient-descent one. Notably, the studies carried out on the SA have confirmed that the trade-off between the bit number and the zoom-step number, that controls the nominal precision, is favorable as already found in the symmetric case [28,29]. Then, a minimal bit number can be chosen, so that the matrix dimension in the QUBO problem does not exceed the current limitations of the quantum hardware. After strengthening our numerical experience on the SA, we performed a numerical campaign by running N_{run} times our algorithm on the D-Wave QA, obtaining very encouraging results. We successfully approached the target eigenpair, extending our studies up to a matrix dimension $n_M = 32$, with a corresponding QUBO-matrix dimension equal to 64. We have shown that the algorithm used in combination with the QA is able to compute the eigenpair corresponding to the largest eigenvalue with 100% reliability and with improvable precision up to $\sim 10^{-8}$. As to the scalability of the algorithm, Table IV yields a promising slightly linear increasing for growing matrix dimension, but more studies have to be performed with larger and larger n_M , before drawing definite conclusions.

With an eye to the future, the next challenge is to improve the algorithm in order to address the generalized eigenvalue problem in its full glory, i.e., without exploiting the nonsingularity of the symmetric matrix.

ACKNOWLEDGMENTS

The Authors gratefully thank *Q@TN—Quantum Science and Technology in Trento*, sponsored by Università degli Studi di Trento, FBK, INFN, CNR and Consorzio Interuniversitario per il Calcolo Automatico dell’Italia del Nord Orientale (CINECA), for providing access and run-time to the CINECA Quantum Computing facility (during the period 2021–2023), where all the numerical results shown in the present work were obtained by using a D-Wave Systems quantum annealer. A. G. acknowledges support from the DOE Topical Collaboration “Nuclear Theory for New Physics,” Award No. DE-SC0023663 and Jefferson Lab that is supported by the U.S. Department of Energy, Office of Nuclear Science, under Contracts No. DE-AC05-06OR23177. During part of the development of this work A. G. was a postdoc at ECT*. T. F. thanks the financial support from CNPq (Conselho Nacional de Desenvolvimento Científico e Tecnológico) Grant No. 306834/2022-7, CAPES (Coordenação de Aperfeiçoamento de Pessoal de Nível Superior), Finance

³A detailed discussion of the heuristic embedding for the three D-Wave topologies: Zephyr (the newest one), Pegasus (the one used for the present calculations), and Chimera (the first topology adopted by D-Wave), can be found in Ref. [64].

⁴In Ref. [26], for *Advantage 4.1*, it is shown that one can reach at most $N_{\text{clique}} = 177$ fully-connected logical bits, with a chain-length equal to 17, while for $N_{\text{clique}} = 647$ the chain length is about 7, not too far from what we found. It should be recalled the critical role of the accuracy one aims to, as well as the condition number of the involved matrices. In our case, the matrix elements, being the outcomes of an actual physical problem, are within an interval several orders of magnitude wide.

Code 001, FAPESP (Grant No. 2019/07767-1) and Instituto Nacional de Ciência e Tecnologia—Física Nuclear e Aplicações Proc. No. 464898/2014-5.

APPENDIX A: THE HOMOGENEOUS BETHE-SALPETER EQUATION

In this appendix, some details about the physical case, which suggested the *nonsymmetric* GEVP to be investigated with the QA, are briefly illustrated.

The Bethe-Salpeter equation (BSE) was introduced [33,34] in order to describe an interacting system within the relativistic quantum-field theory framework (see, e.g., Refs. [35,36] for a detailed introduction). In particular, scattering and bound states can be studied by using inhomogeneous and homogeneous versions of the equation, respectively, in analogy with the Lippmann-Schwinger equation and the Schrödinger one, in the nonrelativistic framework. It should be pointed out that BSE is an integral equation (plus a typical boundary condition in case of the scattering processes), with a kernel constructed through the set of two-particle irreducible Feynman diagrams contributing to the interaction between constituents [33].

The simplest hBSE is the one that allows to dynamically describe a bound system composed by two massive scalars interacting through the exchange of a massive scalar (the case with a simple ladder-exchange of a massless scalar between massless scalars is known as the Wick-Cutkowsky model [65,66]). In 4D Minkowski space, it reads (see Ref. [38] for more details)

$$\Phi_b(k, p) = G_0^{(1)}(k, p) G_0^{(2)}(k, p) \int \frac{d^4 k'}{(2\pi)^4} i\mathcal{K}(k, k', p) \Phi_b(k', p), \quad (\text{A1})$$

where $\Phi_b(k, p)$ is the BS amplitude of a two-body bound system, $p = p_1 + p_2$ the total momentum of the system, with square mass $M^2 = p^2$, $k = (p_1 - p_2)/2$ the relative momentum, and $i\mathcal{K}$ the interaction kernel, that contains all the irreducible diagrams [33]. In Eq. (A1), $G_0^{(i)}(k, p)$ is the free scalar propagator, given by

$$G_0^{(i)}(k, p) = \frac{i}{(\frac{p}{2} \pm k)^2 - m^2 + i\epsilon}, \quad (\text{A2})$$

with m the mass of the scalar constituents.

To proceed for obtaining actual numerical solutions is helpful to adopt the NIR [37,47] of the BS amplitude, so that its analytic structure is made explicit. Within the NIR framework, the BS amplitude is written as a proper folding of (i) a nonsingular weight function that depends upon real variables and appears in the numerator (for the system under consideration, one variable is compact and the other is noncompact), and (ii) a denominator that contains the analytic structure. One writes

$$\Phi_b(k, p) = i \int_{-1}^1 dz' \int_0^\infty d\gamma' \frac{g_b(\gamma', z'; \kappa^2)}{[\gamma' + \kappa^2 - k^2 - p \cdot kz' - i\epsilon]^{2+n}} \quad (\text{A3})$$

where $g_b(\gamma', z'; \kappa^2)$ is the Nakanishi weight function (NWF), $n \geq 1$ is a suitable power that can be chosen with some degree of arbitrariness [37] (one should properly redefine the NWF) and κ^2 is given by

$$\kappa^2 = m^2 - \frac{M^2}{4}, \quad (\text{A4})$$

that is a measure of the binding, defined by $B = 2m - M \geq 0$. Inserting such a relation in Eq. (A4), one gets $\kappa^2 > 0$ for bound states. Interestingly, the dependence upon z' of $g_b(\gamma', z'; \kappa^2)$ is even as expected by the symmetry property of the BS amplitude for the two-scalar system and $g_b(\gamma', z' = \pm 1; \kappa^2) = 0$, as illustrated in Ref. [38]. It is crucial to emphasize that once the NWF is known, then the BS amplitude can be reconstructed via Eq. (A3) and the evaluation physical observables can be carried out.

If the 4D kernel $i\mathcal{K}$ is explicitly known, one can perform the analytic integration of both sides of Eq. (A1). To this end, instead of using the Minkowskian four-momentum k in Cartesian coordinates it is very useful to introduce their light-front (LF) combination, that amount to $k \equiv \{k^\pm = k^0 \pm k^3, \mathbf{k}_\perp\}$ (for interested readers, Ref. [67] yields details on the Dirac proposal of the light-front dynamics, and in general on the relativistic Hamiltonian description of a dynamical system). Hence, one gets an integral equation for the NWF, avoiding the difficulties related to the indefinite metric of the Minkowski space. In particular, the integral equation reads

$$\int_0^\infty d\gamma' \frac{g_b(\gamma', z; \kappa^2)}{[\gamma' + \gamma + z^2 m^2 + (1 - z^2) \kappa^2 - i\epsilon]^2} = \int_0^\infty d\gamma' \int_{-1}^1 dz' V_b^{LF}(\gamma, z; \gamma', z') g_b(\gamma', z'; \kappa^2), \quad (\text{A5})$$

where the new kernel V_b^{LF} , so-called Nakanishi kernel, is related to the 4D BS kernel, $i\mathcal{K}$, in Eq. (A1), as follows

$$V_b^{LF}(\gamma, z; \gamma', z') = ip^+ \int_{-\infty}^\infty \frac{dk^-}{2\pi} G_0^{(1)}(k, p) G_0^{(2)}(k, p) \int \frac{d^4 k'}{(2\pi)^4} \frac{i\mathcal{K}(k, k', p)}{[k'^2 + p \cdot k' z' - \gamma' - \kappa^2 + i\epsilon]^3}, \quad (\text{A6})$$

with $p^+ = M$, once the intrinsic frame where $\mathbf{p}_\perp = 0$ is chosen (one adopts the rest frame for carrying out the calculation, given our interest on the intrinsic properties of the system).

Two comments are in order. Given the dependence on k^2 in both scalar propagators and interaction kernel, one expects double poles in the Cartesian variable k^0 . If one uses LF variables, one remains with single poles in k^- and k^+ , obtaining a simplification in the formal treatment. To numerically evaluate the integral equation (A5), one has to specify the structure of the interaction kernel. A quantitative analysis was carried out by using the exchange of one massive scalar particle, that generates the ladder approximation of the hBSE, by iteration. This means that the integral equation automatically produces an infinite number of scalar exchanges, so that the bound-system pole of the four-leg Green's function can be established. The ladder kernel is given by

$$i\mathcal{K}^{(Ld)}(k, k') = \frac{i(-ig)^2}{(k - k')^2 - \mu^2 + i\epsilon}, \quad (\text{A7})$$

where g is the coupling constant and μ the mass of the exchanged scalar. A quantitative analysis of Eq. (A5) with

the kernel in Eq. (A7) was carried out in Ref. [38] by using a complete orthonormal basis for expanding the NWF $g_b(\gamma, z; \kappa^2)$. In particular, one writes

$$g_b^{(Ld)}(\gamma, z; \kappa^2) = \sum_{\ell=0}^{N_z} \sum_{j=0}^{N_\gamma} \mathcal{C}_{\ell j}(\kappa^2) G_\ell(z) \mathcal{L}_j(\gamma), \quad (\text{A8})$$

where (i) the functions $G_\ell(z)$ are given in terms of even Gegenbauer polynomials, $C_{2\ell}^{(5/2)}(z)$, by

$$G_\ell(z) = 4(1 - z^2)\Gamma(5/2) \sqrt{\frac{(2\ell + 5/2)(2\ell)!}{\pi\Gamma(2\ell + 5)}} C_{2\ell}^{(5/2)}(z), \quad (\text{A9})$$

and (ii) the functions $\mathcal{L}_j(\gamma)$ are expressed in terms of the Laguerre polynomials, $L_j(a\gamma)$, by

$$\mathcal{L}_j(\gamma) = \sqrt{a} L_j(a\gamma) e^{-a\gamma/2}. \quad (\text{A10})$$

The following orthonormality conditions are fulfilled

$$\int_{-1}^1 dz G_\ell(z) G_n(z) = \delta_{\ell n}, \quad \int_0^\infty d\gamma \mathcal{L}_j(\gamma) \mathcal{L}_\ell(\gamma) = a \int_0^\infty d\gamma e^{-a\gamma} L_j(a\gamma) L_\ell(a\gamma) = \delta_{j\ell}. \quad (\text{A11})$$

By inserting the expansion of the NWF and approximating the kernel with only the one-scalar exchange (i.e., the ladder approximation), Eq. (A5) becomes

$$\begin{aligned} & \sum_{\ell' j'} \int_0^\infty d\gamma' \int_{-1}^1 dz \int_0^\infty d\gamma'' \int_{-1}^1 dz' G_{\ell'}(z) \mathcal{L}_{j'}(\gamma) \mathcal{B}(\gamma, z; \gamma', z'; \kappa^2) G_{\ell''}(z') \mathcal{L}_{j''}(\gamma') \mathcal{C}_{\ell' j'}(\kappa^2) \\ & = \alpha \sum_{\ell' j'} \int_0^\infty d\gamma' \int_{-1}^1 dz \int_0^\infty d\gamma'' \int_{-1}^1 dz' G_{\ell'}(z) \mathcal{L}_{j'}(\gamma) \mathcal{V}_b^{Ld}(\gamma, z; \gamma', z') G_{\ell''}(z') \mathcal{L}_{j''}(\gamma') \mathcal{C}_{\ell' j'}(\kappa^2). \end{aligned} \quad (\text{A12})$$

where $\alpha = g^2/(32\pi^2)$, $\mathcal{B}(\gamma, z; \gamma', z'; \kappa^2)$ is a function symmetric under the exchange $\gamma \rightarrow \gamma'$ and $z \rightarrow z'$ given by

$$\mathcal{B}(\gamma, z; \gamma', z'; \kappa^2) = \frac{\delta(z - z')}{[\gamma' + \gamma + z^2 m^2 + (1 - z^2)\kappa^2 - i\epsilon]^2}, \quad (\text{A13})$$

and $\mathcal{V}_b^{Ld}(\gamma, z; \gamma', z')$ is a function nonsymmetric in the above exchange and is obtained from the following integral (see Ref. [38])

$$\mathcal{V}_b^{Ld}(\gamma, z; \gamma', z') = 32\pi p^+ \int_{-\infty}^\infty \frac{dk^-}{2\pi} \int \frac{d^4 k'}{(2\pi)^4} \frac{G_0^{(1)}(k, p) G_0^{(2)}(k, p)}{[(k - k')^2 - \mu^2 + i\epsilon][k'^2 + p \cdot k' z' - \gamma' - \kappa^2 + i\epsilon]^3}. \quad (\text{A14})$$

By applying the above steps, one is able to formally transform the 4D hBSE into a GEVP with the following structure

$$A \mathbf{v}_i = \lambda_i B \mathbf{v}_i, \quad \text{with } i = 1, 2, \dots, n, \quad (\text{A15})$$

where A and B are real square matrices, calculated from rhs and lhs of Eq. (A12) respectively. Moreover, the matrix A is nonsymmetric, while B is symmetric, and they have dimension $n = N_z \times N_\gamma$. The eigenvector \mathbf{v}_i , corresponding to the i th eigenvalue $\lambda_i = 1/\alpha_i$, contains the coefficients

$\mathcal{C}_{\ell_j}(\kappa^2)$ of the expansion of the NWF [cf. Eq. (A8)]. It should be pointed out that the eigenvalues and eigenvectors can be real and complex conjugated, but we are interested only in real eigenvalues, since we aim to describe a physical system (recall that the eigenvalue is the inverse of the square coupling constant, in the ladder approximation we adopted).

APPENDIX B: THE BINARY BASIS

This appendix illustrates how to transform a QUBO problem in a form suitable for the evaluation with a quantum annealer. The needed step is given by the transformation of each component of the involved *real* vectors into their expression in terms of a binary string, by using b *binary variables*. For instance, a generic real number, a , such that $|a| \leq 1$, can be expressed in terms of a binary basis with b bits as follows (see also Refs. [28,29] for details)

$$a = -q_b + q_1 \frac{1}{2} + q_2 \frac{1}{2^2} + q_3 \frac{1}{2^3} + \dots + q_{b-1} \frac{1}{2^{b-1}}, \quad (\text{B1})$$

where $a \in [-1, 1)$ (see below), $q_i = 0, 1$ and the b -th bit carries the sign, i.e., for $a \geq 0$ ($a < 0$) one uses $q_b = 0$ ($q_b = 1$). In a compact form, one can rewrite a as a scalar product between two vectors with b components, viz.

$$a = \mathbf{p}^T \cdot \mathbf{q}_b, \quad (\text{B2})$$

where $\mathbf{q}_b \equiv \{q_1, q_2, \dots, q_b\}$ is a binary string (a column vector in our notation) and $\mathbf{p}^T \equiv \{-1, 1/2, 1/4, \dots,$

$1/2^{b-1}\}$ is a row vector, representing the transpose of the so-called *precision vector*, since $1/2^{b-1}$ controls the precision to which one wants to approximate the number a . Notice that 1 can be reached only asymptotically, since

$$\lim_{b \rightarrow \infty} \sum_{i=1}^{b-1} \frac{1}{2^i} = \frac{1}{2} \lim_{b \rightarrow \infty} \left[\frac{1 - 2^{-(b-1)}}{1/2} \right] \rightarrow 1, \quad (\text{B3})$$

while -1 corresponds to the binary vector $1, 0, \dots, 0$, truncated at any order. Therefore, one has to consider the right-open interval $a \in [-1, 1)$.

One quickly generalizes the compact expression in Eq. (B2) to a vector \mathbf{v} with real components and dimension n , since one has

$$\begin{pmatrix} v_1 \\ v_2 \\ \vdots \\ v_n \end{pmatrix} = \begin{pmatrix} \mathbf{p}^T & 0 & \dots & 0 \\ 0 & \mathbf{p}^T & \dots & 0 \\ \vdots & \vdots & \ddots & 0 \\ 0 & 0 & \dots & \mathbf{p}^T \end{pmatrix} \begin{pmatrix} \mathbf{x}_{1b} \\ \mathbf{x}_{2b} \\ \vdots \\ \mathbf{x}_{nb} \end{pmatrix} = \mathbf{P}^T \mathbf{X}, \quad (\text{B4})$$

where \mathbf{x}_{ib} is the i th binary vector with dimension b . The vector $\mathbf{X} \equiv \{\mathbf{x}_i\}$ in the last line has dimension: $n \times b$, and the rectangular matrix \mathbf{P}^T has n rows and $n \times b$ columns. In the last line $\mathbf{X} \equiv \{\mathbf{x}_i\}$.

Hence, for a $n \times n$ matrix C , and a given vector \mathbf{v} with real components, one can write

$$\begin{aligned} \mathbf{v}^T C \mathbf{v} &= (v_1 \ v_2 \ \dots \ v_n) C \begin{pmatrix} v_1 \\ v_2 \\ \vdots \\ v_n \end{pmatrix} = \begin{pmatrix} \mathbf{x}_{1b}^T & \mathbf{x}_{2b}^T & \dots & \mathbf{x}_{nb}^T \end{pmatrix} \begin{pmatrix} \mathbf{p} & 0 & \dots & 0 \\ 0 & \mathbf{p} & \dots & 0 \\ \vdots & \vdots & \ddots & 0 \\ 0 & 0 & \dots & \mathbf{p} \end{pmatrix} C \begin{pmatrix} \mathbf{p}^T & 0 & \dots & 0 \\ 0 & \mathbf{p}^T & \dots & 0 \\ \vdots & \vdots & \ddots & 0 \\ 0 & 0 & \dots & \mathbf{p}^T \end{pmatrix} \begin{pmatrix} \mathbf{x}_{1b} \\ \mathbf{x}_{2b} \\ \vdots \\ \mathbf{x}_{nb} \end{pmatrix} \\ &= \mathbf{X}^T P C P^T \mathbf{X}, \end{aligned} \quad (\text{B5})$$

recalling that \mathbf{p} is a column vector.

APPENDIX C: INEQUALITIES FOR NONSYMMETRIC-MATRIX EIGENVALUES

In this appendix, some inequalities between the eigenvalues of a $n \times n$ nonsymmetric matrix and the ones of its symmetric part are briefly reviewed, following the results of Ref. [68]. Indeed, in Ref. [68], the most general case of a linear transformation in a n -dimensional unitary space was considered, while we limit ourselves to our specific needs.

Let us introduce the symmetric combination of a real, nonsymmetric matrix A and its transpose A^T

$$S = \frac{A + A^T}{2}. \quad (\text{C1})$$

Recall that $\text{Tr}\{S\} = \sum_i \{\lambda_i(S)\} = \text{Tr}\{A\} = \sum_i \Re e\{\lambda_i(A)\}$ for real A , where $\lambda_i(S)$ (real) and $\lambda_i(A)$ (both real and, possibly, complex conjugated) are the eigenvalues of S and A , with $i = 1, \dots, n$, respectively.

From Theorem II of Ref. [68], one can deduce that the maximal eigenvalue of S is an upper-bound of the maximal eigenvalue of A , as sketched in what follows. It turns out that

$$\sum_{i=1}^q \lambda_i(S) \geq \sum_{i=1}^q \Re e\{\lambda_i(A)\}, \quad \text{with } q \leq n, \quad (\text{C2})$$

where the two sets of eigenvalues are ordered in a decreasing way, i.e., $\lambda_1(S) \geq \lambda_2(S) \geq \dots \geq \lambda_n(S)$ and the same for the real parts of $\lambda_i(A)$. If $q = 1$, then one has the following inequality

$$\lambda_{\max}(S) \geq \Re\{\lambda_{\max}(A)\} \quad (\text{C3})$$

The minimal eigenvalue of S is lower-bound of the minimal eigenvalue of A . Recalling that $\text{Tr}\{A\} = \text{Tr}\{S\}$ one gets

$$\sum_{i=1}^{n-1} \Re\{\lambda_i(A)\} + \Re\{\lambda_{\min}(A)\} = \sum_{i=1}^{n-1} \lambda_i(S) + \lambda_{\min}(S), \quad (\text{C4})$$

and using Eq. (C2) with $q = n - 1$ one eventually has

$$\begin{aligned} \Re\{\lambda_{\min}(A)\} &= \left[\sum_{i=1}^{n-1} \lambda_i(S) - \sum_{i=1}^{n-1} \Re\{\lambda_i(A)\} \right] + \lambda_{\min}(S) \\ &\geq \lambda_{\min}(S). \end{aligned} \quad (\text{C5})$$

It should be pointed out that the antisymmetric combination $\mathcal{A} = (A - A^T)/2$ leads to bounds on the imaginary part of the eigenvalues $\lambda(A)$.

For the sake of completeness, one can mention that if (i) the largest eigenvalue of the symmetric matrix S is positive and (ii) $\lambda_{\max}(A)$ is real and positive, then $\lambda_{\max}(A) = \lambda_{\max}(S)$, after applying Eq. (C3). In fact, by introducing the Schatten p -norm of a matrix M , namely $\|M\|_p = [\text{Tr}\{(M^\dagger M)^{p/2}\}]^{1/p}$ with M^\dagger the Hermitian adjoint (see Ref. [69] for details), one has

$$\|S\|_p \leq \|A\|_p = \|A^T\|_p \quad \forall p. \quad (\text{C6})$$

Notice the difference with the ℓ_p -norm given by $\|M\|_p = \sup_{\|\mathbf{x}\|_p=1} \|M\mathbf{x}\|_p$, although these two norms share the same notation. It turns out that the Schatten p -norm becomes the spectral norms (that amount to ℓ_2 norms) for $p = \infty$ [69], and therefore in this limit Eq. (C6) reads

$$\begin{aligned} \|S\|_\infty &= \max [|\lambda_{\min}(S)|, |\lambda_{\max}(S)|] \\ &\leq \max [|\lambda_{\min}(A)|, |\lambda_{\max}(A)|] = \|A\|_\infty, \end{aligned} \quad (\text{C7})$$

where the standard spectral norm is given by the largest $|\lambda|$. Since we have assumed that the symmetric matrix S has a positive largest eigenvalue, one can readily write

$$\|S\|_\infty = \lambda_{\max}(S) \leq |\lambda_{\max}(A)| = \|A\|_\infty \quad (\text{C8})$$

and after taking into account Eq. (C3) one writes

$$\begin{aligned} \Re\{\lambda_{\max}(A)\}^2 &\leq \lambda_{\max}(S)^2 \leq |\lambda_{\max}(A)|^2 \\ &= \Re\{\lambda_{\max}(A)\}^2 + \Im\{\lambda_{\max}(A)\}^2 \end{aligned} \quad (\text{C9})$$

This means that if the largest eigenvalue of A is real then the largest eigenvalue of S will be equal to it. Unfortunately the

assumptions are quite restrictive and are not fulfilled by our actual matrices.

For the symmetric combination AA^T , one has an analogous result. For the sake of simplicity (and since we are interested in), we focus on real eigenvalues of the non-symmetric matrix A . One writes

$$A\mathbf{x}_{\lambda(A)} = \lambda(A)\mathbf{x}_{\lambda(A)}, \quad \mathbf{x}_{\lambda(A)}^T A^T = \lambda(A)\mathbf{x}_{\lambda(A)}^T \quad (\text{C10})$$

and

$$\mathbf{x}_{\lambda(A)}^T A^T A \mathbf{x}_{\lambda(A)} = \lambda^2(A)\mathbf{x}_{\lambda(A)}^T \mathbf{x}_{\lambda(A)}. \quad (\text{C11})$$

Let us now consider the eigenvalue problem for the symmetric matrix $P = A^T A$. One has real eigenvalues and eigenvectors generating an orthonormal basis. To establish formalism, one writes

$$P\mathbf{x}_{\lambda_i(P)} = \lambda_i(P)\mathbf{x}_{\lambda_i(P)}. \quad (\text{C12})$$

The expansion of an eigenvector of A on the orthonormal basis $\mathbf{x}_{\lambda_i(P)}$ yields

$$\mathbf{x}_{\lambda(A)} = \sum_i c_i \mathbf{x}_{\lambda_i(P)}$$

that leads to

$$\begin{aligned} \mathbf{x}_{\lambda(A)}^T A^T A \mathbf{x}_{\lambda(A)} &= [\lambda(A)]^2 \\ &= \sum_i \lambda_i(P) c_i^2 |\mathbf{x}_{\lambda_i(P)}^T \mathbf{x}_{\lambda(A)}|^2 \\ &\geq \lambda_{\min}(P) \mathbf{x}_{\lambda(A)}^T \mathbf{x}_{\lambda(A)}, \end{aligned} \quad (\text{C13})$$

and then

$$\lambda_{\max}(P) \geq [\lambda(A)]^2 \geq \lambda_{\min}(P), \quad (\text{C14})$$

where an obvious inequality involving $\lambda_{\max}(P)$ has been used for the lhs. In conclusion, again the minimal(maximal) eigenvalue of the naively symmetrized matrix is a lower (upper) bound, and a variational method can return $\lambda_{\min}(P)$ ($\lambda_{\max}(P)$) and not $\lambda(A)$.

Another possible approach to be mentioned is based on the following symmetric form

$$\tilde{A} = \begin{pmatrix} 0 & A \\ A^T & 0 \end{pmatrix}. \quad (\text{C15})$$

Since the nonsymmetric matrices A and its transpose has the same set of eigenvalues but not the right, or left, eigenvectors one should solve the following *symmetric* GEPV

$$\begin{pmatrix} 0 & A \\ A^T & 0 \end{pmatrix} \begin{pmatrix} \mathbf{w}_i \\ \mathbf{v}_i \end{pmatrix} = \lambda_i \begin{pmatrix} 0 & 1 \\ 1 & 0 \end{pmatrix} \begin{pmatrix} \mathbf{w}_i \\ \mathbf{v}_i \end{pmatrix} \quad (\text{C16})$$

where $A\mathbf{v}_i = \lambda_i\mathbf{v}_i$ and $A^T\mathbf{w}_i = \lambda_i\mathbf{w}_i$. Clearly, this approach doubles the dimension of the initial problem and therefore is confronted with the limits of the matrix dimension tractable by using a quantum annealer.

- [1] J. Preskill, Quantum computing in the NISQ era and beyond, *Quantum* **2**, 79 (2018).
- [2] J. Preskill, The physics of quantum information, [arXiv:2208.08064](https://arxiv.org/abs/2208.08064).
- [3] C. W. Bauer *et al.*, Quantum simulation for high-energy physics, *PRX Quantum* **4**, 027001 (2023).
- [4] L. Funcke, T. Hartung, K. Jansen, and S. Kühn, Review on quantum computing for lattice field theory, *Proc. Sci. LATTICE2022* (2023) 228.
- [5] A. Delgado *et al.*, Quantum computing for data analysis in high energy physics, [arXiv:2203.08805](https://arxiv.org/abs/2203.08805).
- [6] Y. Cao, J. Romero, J. P. Olson, M. Degroote, P. D. Johnson, M. Kieferová, I. D. Kivlichan, T. Menke, B. Peropadre, N. P. Sawaya *et al.*, Quantum chemistry in the age of quantum computing, *Chem. Rev.* **119**, 10856 (2019).
- [7] B. Bauer, S. Bravyi, M. Motta, and G. K.-L. Chan, Quantum algorithms for quantum chemistry and quantum materials science, *Chem. Rev.* **120**, 12685 (2020).
- [8] P. S. Emani, J. Warrell, A. Anticevic, S. Bekiranov, M. Gandal, M. J. McConnell, G. Sapiro, A. Aspuru-Guzik, J. T. Baker, M. Bastiani *et al.*, Quantum computing at the frontiers of biological sciences, *Nat. Methods* **18**, 701 (2021).
- [9] F. F. Flöther, The state of quantum computing applications in health and medicine, [arXiv:2301.09106](https://arxiv.org/abs/2301.09106).
- [10] F. Bova, A. Goldfarb, and R. G. Melko, Commercial applications of quantum computing, *Eur. Phys. J. Quantum Technol.* **8**, 2 (2021).
- [11] D. Herman, C. Googin, X. Liu, A. Galda, I. Safro, Y. Sun, M. Pistoia, and Y. Alexeev, A survey of quantum computing for finance, [arXiv:2201.02773](https://arxiv.org/abs/2201.02773).
- [12] B. Cheng *et al.*, Noisy intermediate-scale quantum computers, *Front. Phys.* **18**, 21308 (2023).
- [13] Y. Alexeev *et al.*, Quantum computer systems for scientific discovery, *PRX Quantum* **2**, 017001 (2021).
- [14] Y. Kim, A. Eddins, S. Anand, K. X. Wei, E. Van Den Berg, S. Rosenblatt, H. Nayfeh, Y. Wu, M. Zaletel, K. Temme *et al.*, Evidence for the utility of quantum computing before fault tolerance, *Nature (London)* **618**, 500 (2023).
- [15] A. B. Finnila, M. A. Gomez, C. Sebenik, C. Stenson, and J. D. Doll, Quantum annealing: A new method for minimizing multidimensional functions, *Chem. Phys. Lett.* **219**, 343 (1994).
- [16] T. Kadowaki and H. Nishimori, Quantum annealing in the transverse Ising model, *Phys. Rev. E* **58**, 5355 (1998).
- [17] S. Morita and H. Nishimori, Mathematical foundation of quantum annealing, *J. Math. Phys. (N.Y.)* **49** (2008).
- [18] G. E. Santoro and E. Tosatti, Optimization using quantum mechanics: Quantum annealing through adiabatic evolution, *J. Phys. A* **39**, R393 (2006).
- [19] A. Das and B. K. Chakrabarti, Colloquium: Quantum annealing and analog quantum computation, *Rev. Mod. Phys.* **80**, 1061 (2008).
- [20] C. Baldassi and R. Zecchina, Efficiency of quantum vs. classical annealing in nonconvex learning problems, *Proc. Natl. Acad. Sci. U.S.A.* **115**, 1457 (2018).
- [21] P. Hauke, H. G. Katzgraber, W. Lechner, H. Nishimori, and W. D. Oliver, Perspectives of quantum annealing: Methods and implementations, *Rep. Prog. Phys.* **83**, 054401 (2020).
- [22] S. Abel, A. Blance, and M. Spannowsky, Quantum optimization of complex systems with a quantum annealer, *Phys. Rev. A* **106**, 042607 (2022).
- [23] A. D. King *et al.*, Quantum critical dynamics in a 5,000-qubit programmable spin glass, *Nature (London)* **617**, 61 (2023).
- [24] A. Rajak, S. Suzuki, A. Dutta, and B. K. Chakrabarti, Quantum annealing: An overview, *Phil. Trans. R. Soc. A* **381**, 20210417 (2023).
- [25] C. McGeoch and P. Farré, The D-Wave Advantage System: An overview, D-Wave Technical Report No. 14-1049A-A, 2020.
- [26] C. McGeoch and P. Farré, The advantage system: performance update, D-Wave Technical Report No. 14-1054A-A, 2021.
- [27] C. McGeoch and P. Farré, Advantage processor overview, D-Wave Technical Report No. 14-1058A-A, 2022.
- [28] B. Krakoff, S. M. Mniszewski, and C. F. A. Negre, A QUBO algorithm to compute eigenvectors of symmetric matrices, [arXiv:2104.11311](https://arxiv.org/abs/2104.11311).
- [29] B. Krakoff, S. M. Mniszewski, and C. F. Negre, Controlled precision qubo-based algorithm to compute eigenvectors of symmetric matrices, *PLoS One* **17**, e0267954 (2022).
- [30] M. Illa and M. J. Savage, Basic elements for simulations of standard-model physics with quantum annealers: Multigrid and clock states, *Phys. Rev. A* **106**, 052605 (2022).
- [31] G. Tosti Balducci, B. Chen, M. Möller, M. Gerritsma, and R. De Breuker, Review and perspectives in quantum computing for partial differential equations in structural mechanics, *Front. Mech. Eng.* **8**, 914241 (2022).
- [32] A. Stockley and K. Briggs, Optimizing antenna beamforming with quantum computing, in *Proceedings of the 2023 17th European Conference on Antennas and Propagation (EuCAP)* (IEEE, New York, 2023), pp. 1–5.
- [33] E. E. Salpeter and H. A. Bethe, A relativistic equation for bound-state problems, *Phys. Rev.* **84**, 1232 (1951).
- [34] M. Gell-Mann and F. Low, Bound states in quantum field theory, *Phys. Rev.* **84**, 350 (1951).
- [35] C. Itzykson and J.-B. Zuber, *Quantum Field Theory* (Courier Corporation, North Chelmsford, MA, 2012).
- [36] N. Nakanishi, A general survey of the theory of the Bethe-Salpeter equation, *Prog. Theor. Phys. Suppl.* **43**, 1 (1969).
- [37] N. Nakanishi, *Graph Theory and Feynman Integrals* (Gordon and Breach, New York, 1971).
- [38] T. Frederico, G. Salmè, and M. Viviani, Quantitative studies of the homogeneous Bethe-Salpeter equation in Minkowski space, *Phys. Rev. D* **89**, 016010 (2014).
- [39] S. Alliney, F. Laudiero, and M. Savoia, A variational technique for the computation of the vibration frequencies of mechanical systems governed by nonsymmetric matrices, *Appl. Math. Model.* **16**, 148 (1992).
- [40] N.-I. Kim, D. K. Shin, and M.-Y. Kim, Improved flexural-torsional stability analysis of thin-walled composite beam and exact stiffness matrix, *Int. J. Mech. Sci.* **49**, 950 (2007).
- [41] C. Li and C. Vuik, Eigenvalue analysis of the simple preconditioning for incompressible flow, *Numer. Linear Algebra Appl.* **11**, 511 (2004).
- [42] F. Scheben and I. G. Graham, Iterative methods for neutron transport eigenvalue problems, *SIAM J. Sci. Comput.* **33**, 2785 (2011).

- [43] E. A. Burroughs, L. A. Romero, R. B. Lehoucq, and A. G. Salinger, Linear stability of flow in a differentially heated cavity via large-scale eigenvalue calculations, *Int. J. Numer. Methods Heat Fluid Flow* **14**, 803 (2004).
- [44] K. Orginos and D. Richards, Improved methods for the study of hadronic physics from lattice QCD, *J. Phys. G* **42**, 034011 (2015).
- [45] S. Yarkoni, E. Raponi, T. Bäck, and S. Schmitt, Quantum annealing for industry applications: Introduction and review, *Rep. Prog. Phys.* **85**, 104001 (2022).
- [46] M. W. Johnson, M. H. Amin, S. Gildert, T. Lanting, F. Hamze, N. Dickson, R. Harris, A. J. Berkley, J. Johansson, P. Bunyk *et al.*, Quantum annealing with manufactured spins, *Nature (London)* **473**, 194 (2011).
- [47] N. Nakanishi, Partial-wave Bethe-Salpeter equation, *Phys. Rev.* **130**, 1230 (1963).
- [48] C. D. Roberts and A. G. Williams, Dyson-Schwinger equations and their application to hadronic physics, *Prog. Part. Nucl. Phys.* **33**, 477 (1994).
- [49] P. Maris and C. D. Roberts, Dyson-Schwinger equations: A tool for hadron physics, *Int. J. Mod. Phys. E* **12**, 297 (2003).
- [50] A. Bashir, L. Chang, I. C. Cloët, B. El-Bennich, Y.-X. Liu, C. D. Roberts, and P. C. Tandy, Collective perspective on advances in Dyson-Schwinger equation QCD, *Commun. Theor. Phys.* **58**, 79 (2012).
- [51] K. Osterwalder and R. Schrader, Axioms for Euclidean Green's functions, *Commun. Math. Phys.* **31**, 83 (1973).
- [52] K. Osterwalder and R. Schrader, Axioms for Euclidean Green's functions. 2., *Commun. Math. Phys.* **42**, 281 (1975).
- [53] F. Glover, G. Kochenberger, and Y. Du, A tutorial on formulating and using QUBO models, [arXiv:1811.11538](https://arxiv.org/abs/1811.11538).
- [54] A. Teplukhin, B. K. Kendrick, and D. Babikov, Calculation of molecular vibrational spectra on a quantum annealer, *J. Chem. Theory Comput.* **15**, 4555 (2019).
- [55] D. Pastorello and E. Blanzieri, Quantum annealing learning search for solving QUBO problems, *Quantum Inf. Process.* **18**, 1 (2019).
- [56] A. Teplukhin, B. K. Kendrick, and D. Babikov, Solving complex eigenvalue problems on a quantum annealer with applications to quantum scattering resonances, *Phys. Chem. Chem. Phys.* **22**, 26136 (2020).
- [57] C. C. Chang, A. Gambhir, T. S. Humble, and S. Sota, Quantum annealing for systems of polynomial equations, *Sci. Rep.* **9**, 10258 (2019).
- [58] H. Wolkowicz and G. P. Styan, Bounds for eigenvalues using traces, *Linear Algebra Appl.* **29**, 471 (1980).
- [59] R. S. Varga, *Geršgorin and His Circles* (Springer Science & Business Media, Berlin, 2010), Vol. 36.
- [60] E. Anderson, Z. Bai, C. Bischof, S. Blackford, J. D. J. Dongarra, J. D. Croz, A. Greenbaum, S. Hammarling, A. McKenney, and D. Sorensen, *LAPACK Users' Guide*, 3rd ed. (SIAM, Philadelphia, Pennsylvania, USA, 1999).
- [61] P. Date, R. Patton, C. Schuman, and T. Potok, Efficiently embedding QUBO problems on adiabatic quantum computers, *Quantum Inf. Process.* **18**, 117 (2019).
- [62] S. Okada, M. Ohzeki, M. Terabe, and S. Taguchi, Improving solutions by embedding larger subproblems in a D-Wave quantum annealer, *Sci. Rep.* **9**, 2098 (2019).
- [63] J. Cai, W. G. Macready, and A. Roy, A practical heuristic for finding graph minors, [arXiv:1406.2741](https://arxiv.org/abs/1406.2741).
- [64] K. Boothby, A. D. King, and J. Raymond, Zephyr topology of D-Wave quantum processors, D-Wave Technical Report No. 14-1056A-A, 2021.
- [65] G. C. Wick, Properties of Bethe-Salpeter wave functions, *Phys. Rev.* **96**, 1124 (1954).
- [66] R. E. Cutkosky, Solutions of a Bethe-Salpeter equations, *Phys. Rev.* **96**, 1135 (1954).
- [67] P. A. M. Dirac, Forms of relativistic dynamics, *Rev. Mod. Phys.* **21**, 392 (1949).
- [68] K. Fan, On a theorem of Weyl concerning eigenvalues of linear transformation: II, *Proc. Natl. Acad. Sci. U.S.A.* **36**, 31 (1950).
- [69] R. Bhatia, *Matrix Analysis* (Springer, New York, NY, 2012).